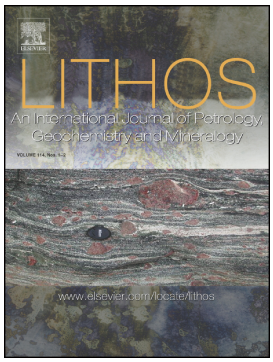

Petrogenesis of Cretaceous (133–84Ma) intermediate dykes and host granites in southeastern China: Implications for lithospheric extension, continental crustal growth, and geodynamics of Palaeo-Pacific subduction

Jinbao Yang, Zhidan Zhao, Qingye Hou, YaolingNiu, Xuanxue Mo, Dan Sheng, Lili Wang

PII: S0024-4937(17)30373-0
DOI: doi:10.1016/j.lithos.2017.10.022
Reference: LITHOS 4459

To appear in:

Received date: 17 August 2017
Accepted date: 29 October 2017

Please cite this article as: Jinbao Yang, Zhidan Zhao, Qingye Hou, YaolingNiu, Xuanxue Mo, Dan Sheng, Lili Wang , Petrogenesis of Cretaceous (133–84Ma) intermediate dykes and host granites in southeastern China: Implications for lithospheric extension, continental crustal growth, and geodynamics of Palaeo-Pacific subduction. The address for the corresponding author was captured as affiliation for all authors. Please check if appropriate. Lithos(2017), doi:10.1016/j.lithos.2017.10.022

Petrogenesis of Cretaceous (133-84 Ma) intermediate dykes and host granites in southeastern China: Implications for lithospheric extension, continental crustal growth, and geodynamics of Palaeo-Pacific subduction

Jinbao Yang [a, b], Zhidan Zhao [a, *], Qingye Hou [a], YaolingNiu [a, c, d], Xuanxue Mo [a], Dan Sheng [e], Lili Wang [a]

[a] *State Key Laboratory of Geological Processes and Mineral Resources, and School of Earth Science and Mineral Resources, China University of Geosciences, Beijing 100083, China*

[b] *Collaborative Innovation Center for Exploration of Hidden Nonferrous Metal Deposits and Development of New Materials in Guangxi, Guangxi Key Laboratory of Hidden Metallic Ore Deposits Exploration, College of Earth Sciences, Guilin University of Technology, Guilin 541006, China*

[c] *Laboratory for Marine Geology, Qingdao National Laboratory for Marine Science and Technology, Qingdao 266061, China*

[d] *Department of Earth Sciences, Durham University, Durham DH1 3LE, UK*

[e] *Hunan Land and Resources Planning Institute, Changsha 410007, China*

*Corresponding author. Division of Petrology and Mineralogy, School of Earth Science and Mineral Resources, China University of Geosciences, 29 Xueyuan Road, Haidian District, Beijing 100083, China. E-mail address: zdzhao@cugb.edu.cn (**Zhidan Zhao**)

Abstract

This paper presents U-Pb zircon geochronology, petrology, and major and trace element, Sr-Nd and zircon Hf isotopic geochemistry of Cretaceous granites and intermediate dykes in the Quanzhou and Xiamen regions of southeastern China. These data are used to investigate igneous petrogenesis and Cretaceous tectonic evolution, and interpret the geodynamics of Palaeo-Pacific slab subduction. Granites in Quanzhou and Xiamen range in age from 133 Ma to 87 Ma, have high SiO_2 and K_2O contents, low abundances in P_2O_5, and an A/CNK index that ranges from 0.97 to 1.09, indicating that they are high-K calc-alkaline metaluminous I-type rocks. Slightly negative $\varepsilon_{Nd}(t)$ values (-1.2 to -4.4), young Nd model ages (0.87 Ga to 1.20 Ga) and positive $\varepsilon_{Hf}(t)$ values (-0.5 to +9.9) of zircon grains indicate that the granites were derived from magmas that melted amphibolite in the middle-lower crust, and which may have assimilated country rocks during emplacement in shallow chambers. The intermediate dykes have no genetic link to the granites and magma mixing was negligible. Eight dyke samples have low SiO_2 and high MgO, Ni and Cr contents. Negative $\varepsilon_{Nd}(t)$ values (-1.5 to -2.7) and positive $\varepsilon_{Hf}(t)$ values (2.7 to 7.6) suggest that the dykes were derived from residual basic lower crust after mafic-crystal accumulation. Two samples of adakite-like dykes are characterised by high Sr/Y ratios (89 to 100) and high SiO_2low K_2O, Ni, Cr contents. In combination with slightly negative $\varepsilon_{Nd}(t)$ values (-1.7 to -1.8) and positive $\varepsilon_{Hf}(t)$ values (2.9 to 4.3), the adakite-like dykes were derived from cumulate basic lower crust which had a mixed source between depleted mantle- and crust-derived melts. Based on our data, combined with previously published work, we suggest that extension-induced middle-lower crustal melting and underplating of mantle-derived basaltic melts were the principal driving mechanisms for Cretaceous granitic magmatism in coastal Fujian Province. Extension was

related to subduction retreat whereas steep slab subduction caused underplating of mantle-derived basaltic melts. These processes were coupled and mainly responsible for the tectonic transition during the Cretaceous from compression to extension in the coastal belt of the Cathaysia Plate.

Key words: Cretaceous; Granite; Dyke; Petrogenesis; Subduction; Southeastern China

1. Introduction

Granites have long been recognised to play a central role in the evolution and growth of continental crust, whereas basic-intermediate dykes are key elements in understanding subduction-related geodynamic processes. It is commonly suggested that mantle-derived magmas play a prominent role in the origin of granitoids (Annen and Sparks, 2002; Bergantz, 1989; Huppert and Sparks, 1988; Petford and Gallagher, 2001), for example by the partial melting of the mantle wedge, triggered by fluids from the subducting oceanic slab, or of underplated basaltic magma.

Granites of various ages are distributed throughout southeastern China, but Mesozoic granites of the Cathaysia Plate (Fig. 1) in particular have provided important constraints on petrogenetic models of Palaeo-Pacific slab subduction (e.g., Jahn *et al.*, 1990; Klimetz, 1983; Li and Li, 2007; Li *et al.*, 2007; Li *et al.*, 2014; Meng *et al.*, 2012; Niu, 2014; Zhou and Li, 2000; Zhou *et al.*, 2006). However, these subduction-based models, are controversial because there is a range of hypotheses, namely normal subduction (Jahn *et al.*, 1990; Klimetz, 1983), flat-slab subduction (Li and Li, 2007; Li *et al.*, 2007; Meng *et al.*, 2012), changing-angle subduction (Zhou and Li, 2000) and subduction retreat (Niu, 2014). Most research has focused on Cretaceous granites of the coastal Fujian Province (e.g., Chen *et al.*, 2004; Chen *et al.*, 2013, 2014; Li *et al.*, 2012a; Qiu *et al.*, 2012; Zhao *et al.*, 2012). The study by Dong *et al.*

(2011), that only discussed the temporal and spatial relationships between two mafic dykes and host granites, and is therefore deficient despite there being an established spatial relationship between mafic dykes and the granites. In contrast, there has been little research on granites of the Quanzhou and Xiamen regions (Li *et al.*, 2012a).

The purpose of this paper is to document the evolution of the coastal granitoid belt using high quality U-Pb zircon dating and zircon Hf isotopic analyses, bulk-rock major and trace-element compositions, and Sr-Nd isotopic analyses of basic-intermediate dykes and their host granites in Quanzhou and Xiamen, in order to improve our understanding of the nature of the middle-lower crust and Cretaceous crust-mantle interaction in coastal Fujian Province, southeastern China. Complementing previous studies, this study highlights the temporal and spatial distribution of Cretaceous magmatism and the significant subduction polarity of crustal rocks upon the subducted Palaeo-Pacific slab, and provides an enhanced understanding of Cretaceous lithospheric extension, crustal growth, and trench/subduction retreat.

2. Regional geology

The South China Block (SCB) comprises the Yangtze Craton in the northwest and the Cathaysia Block in the southeast (Fig. 1), which are separated by the Shaoxing-Jiangshan-Pingxiang Fault Zone(SJPF) (Shu *et al.*, 2009; Wang and Shu, 2012) and characterised by multistage tectono-magmatic events (Jahn, 1974; Zhou and Li, 2000; Zhou *et al.*, 2006). Mesozoic igneous rocks are predominately distributed in the part of the Cathaysia Block that was referred to by Zhou *et al.* (2006) as "the southeast region of the SCB (SE-SCB)", with a total outcrop area of nearly 218,090 km^2, and outcrop-area percentages of granitoids versus volcanic rocks of respectively 58.4% (127,300 km^2) and 41.6% (90,790 km^2). More

than 90%of Mesozoic magmatic rocks in the SE-SCB are felsic in composition, with only a small volume being basic. Mesozoic magmatism significantly increases in volume and becomes younger from inland to coastal regions (Zhou *et al*., 2006; Zhou, 2007).

Six large-scale fault zones (FZs)cross the SE-SCB (Fig. 1), namely: 1) the NE-trending Changle-Nan'ao FZ (CNF), 2) the NE-trending Zhenghe-Dapu FZ (ZDF), 3) the close-to NS-trending Ganjiang FZ (GF), 4) the NE-trending Sihui-Wuchuan FZ (SWF) (Shu *et al*., 2009), 5) the NE-trending Guangchang-Xunwu FZ (GXF), and 6) the NE-trending Ningyuan-Jianghua FZ (NJF) (Zheng *et al*., 2004). The GF is a sinistral fault whereas the CNF is a sinistral ductile shear. Shear deformation associated with the CNF has been dated at 120-100 Ma, by $^{40}Ar/^{39}Ar$ on muscovite from mica-schist (Wang and Lu, 2000), and is related to oblique subduction of the Kula Plate (Palaeo-Pacific) (Charvet *et al*., 1994; Tong and Tobisch, 1996). Seismic tomographic studies have shown that a stagnant Palaeo-Pacific slab is clearly visible in cross sections at 600 km depth below East China, whereas the transition zone beneath the upper mantle of the Fujian coastal region and the Taiwan Strait has low P-wave velocity (low-Vp) (Huang and Zhao, 2006). High-Vp materials under Taiwan have penetrated the mantle transition zone and entered the lower mantle. Low-Vp anomalies under the SE-SCB and the Philippine Sea may represent mantle upwelling flow driven by deep slab subduction (Zhao, 2004a; Huang *et al*., 2010).

The Fujian Province is located within the SE-SCB, and is subdivided by the ZDF into a western part, which is mostly covered by Middle-Late Jurassic granites and minor Triassic granites, and an eastern part, in which Cretaceous granites and volcanic rocks dominate (Fig. 1). Voluminous Early Palaeozoic and Triassic per-aluminous (usually S-type) granites and some I-type granites are exposed in the western Fujian Province. These granites are

interpreted to be responses to the tectonic change from compressive to local post-collisional extensional regimes associated respectively with Caledonian and Indosinian orogenesis (Li *et al.*, 2012b; Zhou *et al.*, 2006). In contrast, an extensional tectonic regime prevailed in Fujian Province at the same time, whereas extension- and arc-related magmatism (e.g., bimodal volcanic rocks and A-type granites) occurred during the Jurassic-Cretaceous. Despite a long-standing controversy on the Late Mesozoic tectono-magmatic evolution of the area, the regional geodynamic setting is generally regarded to have been an active continental margin associated with subduction of a Palaeo-Pacific slab (Li *et al.*, 2007; Li *et al.*, 2014; Wang *et al.* 2013; Zhou and Li, 2000; Zhou and Chen, 2001; Zhou *et al.*, 2006).

3. Field observation and petrography

This study focuses on the Mesozoic granites and intermediate dykes of the Quanzhou and Xiamen regions, which are located in coastal Fujian Province and includes the Zhangban, Huian, Sidu, Damaoshan and Xiamen (i.e., Xiamen Island) plutons (Fig. 1; Fig. 2a, b). The plutons in Quanzhou have a total exposed area of ~600 km^2 (Fig. 2a), are intruded by intermediate dykes (Fig. 2d), and comprise monzogranite, fine-grained granite, biotite-bearing granite, and minor granite porphyry. The Xiamen Pluton (~60 km^2) is composed mainly of monzogranite and biotite-bearing granite (Fig. 2b), and is intruded by near-vertical intermediate dykes (Fig. 2c). All the sampled dykes have a NE-trending strike, parallel to the coastline, as also described by Chen *et al.* (2002). Furthermore, there are minor gabbroic intrusions, widespread dynamic-metamorphic rocks (T-J), and late Jurassic intermediate-felsic pyroclastic and volcaniclastic rocks interlayered with mudstone, sandstone, and siliceous rocks (J_{3n}^{b-c}) in both regions (Fig. 2a, b) (e.g., in Houzhu and Songyu). The dynamic-metamorphic rocks (T-J) are leptynite, which is composed of biotite, plagioclase,

K-feldspar, and quartz, and interpreted to have originally been intermediate-felsic volcanic or volcaniclastic rock (FJBGMR, 1985).

Thirty-three samples were collected from the two study areas, comprising ten intermediate dykes and twenty-three granite plutons. Porphyritic intermediate rocks are characterised mainly by distinctive sets of phenocrysts. Dioritic porphyrites have a phenocryst assemblage of plagioclase (~60%), hornblende (~35%) and quartz (<5%) (Fig. 3a), whereas some sample shave euhedral phenocrysts of sanidine (Fig. 3b). Gabbroic dioritic porphyries contain calcite amygdales and phenocrysts of clinopyroxene and plagioclase set in a glassy groundmass (Fig. 3c). Granite porphyry is characterised by phenocrysts of quartz (~50%), with embayed grain boundaries suggesting resorption, and of plagioclase (~45%), with oscillatory concentric zoning, and biotite (~5%) (Fig. 3d). Biotite-bearing granite is composed of K-feldspar (25% to 30%), plagioclase (30% to 35%), quartz (~25%), biotite (~4%), and muscovite (~3%) with minor zircon and Fe-Ti oxides (Fig. 3e). Monzogranite mainly comprises K-feldspar (35% to 40%), plagioclase (30% to 35%),with common oscillatory zoning, quartz (~25%), and biotite (~5%), whereas K- and Na-feldspars occasionally occur as perthite (Fig. 3f, g). Fine-grained granite is composed of plagioclase (~30%), K-feldspar (~35%), quartz (~25%), biotite (<5%) and muscovite (<5%) (Fig. 3h, i). No granites have obvious apatite crystals in thin sections.

4. Analytical methods

4.1 LA-ICP-MS U-Pb zircon dating

Nine granite samples and three dyke samples were selected for U-Pb zircon dating. Zircon grains were separated via gravity, magnetic, heavy liquid separation techniques in the

Laboratory of the Geological Team of Hebei Province, China. Cathodoluminescence (CL) images were obtained at the Institute of Geology and Geophysics, Chinese Academy of Sciences (IGGCAS), to examine the internal structure of individual zircon grains, and for the selection of sites for zircon isotope analyses.

Uranium-Pb zircon dating was performed by LA-ICP-MS at the State Key Laboratory of Geological Processes and Mineral Resources (GPMR), China University of Geosciences, Wuhan, China. Detailed operating conditions for the laser ablation system and the ICP-MS instrument, and data reduction are identical to those described by Liu *et al*. (2008a, 2010b). Laser sampling was performed using a GeoLas 2005 (Lambda Physik, Göttingen, Germany). An Agilent 7500a ICP-MS instrument (Agilent Technologies Inc., Japan) was used to acquire ion-signal intensities. The off-line selection and integration of background and analysis signals, the time-drift correction, and the U-Pb dating were performed by *ICPMSDataCal* (Liu *et al*., 2008a, 2010b).

Zircon grain 91500 was used as an external standard for the U-Pb dating and was analysed twice every five analyses. Time-dependent drifts of the U-Th-Pb isotopic ratios were corrected using a linear interpolation (with time) for every five analyses according to the variations of the zircon grain 91500 (i.e., 2 zircon grains of 91500 + 6 samples + 2 zircon grains of 91500) (Liu *et al*., 2010b). The preferred U-Th-Pb isotopic ratios used for zircon grain 91500 are from Wiedenbeck *et al*. (1995). The uncertainty of preferred values for the external standard zircon grain 91500 was propagated to the final results from the samples. Common lead was corrected for using the correction function of Andersen (2002). The program *ISOPLOT* (version 3.0) (Ludwig, 2003) was used for plotting Concordia diagrams and age spectra, and for age calculations. Uncertainties in individual analyses are reported at1σ;

weighted mean ages for pooled $^{206}Pb/^{238}U$ results are reported at2σ. The U-Pbzircon isotopic data are presented in Table S1.

4.2Major and trace elements geochemical analyses

Bulk-rock major element compositions were determined by inductive coupled plasma-atomic emission spectroscopy (ICP-AES) (Prodigy)at the GPMR, China University of Geosciences, Beijing. Operating procedures are described by Song *et al*. (2010). The reproducibility deduced from replicate analyses is typically better than 1% with the exception of TiO_2 (~1.5%) and P_2O_5 (~2.0%). Trace-element compositions (including rare earth elements) were analysed by ICP-MS (Agilent 7500a) after sample powders were digested by HF and HNO_3 in Teflon bombs at the GPMR, China University of Geosciences, Wuhan, China. The detailed sample-digesting procedure for ICP-MS analyses and analytical precision and accuracy for trace elements are as presented by Liu *et al*. (2008b). Major and trace element geochemical data are presented in Table S2.

4.3 Bulk-rock Rb-Sr and Sm-Nd isotopic analyses

Bulk-rock Sr and Nd isotopic compositions were determined using a Finnigan MAT-261 multi-collector mass spectrometer operated in static mode at GPMR, China University of Geosciences, Wuhan, China. Analytical details are given in Liu *et al*. (2004) and Rudnick *et al*. (2004). Sr and Nd isotopic fractionation was normalised respectively to $^{86}Sr/^{88}Sr = 0.11940$ and $^{146}Nd/^{144}Nd = 0.721900$. The average $^{143}Nd/^{144}Nd$ ratio of the JNdi-1 standard (Geological Survey of Japan) measured during the sample runs is 0.512106 ± 7(2σ, n = 8), and the average $^{87}Sr/^{86}Sr$ ratio of the NBS987 standard (US National Institute of Standards and Technology) is 0.710249 ± 9(2σ, n = 8). Total procedural Sr and Nd blanks are respectively <1

ng and <50 pg. The Sr-Nd isotopic data are presented in Table S3.

4.4 In situ zircon Hf isotope analyses

Hafnium isotopic measurements were performed on the same spots or the same age domains used for age determinations of concordant grains, as guided by CL images. Analyses were conducted using a Neptune Plus MC-ICP-MS (Thermo Fisher Scientific, Germany) in combination with a Geolas 2005 excimer ArF laser ablation system (Lambda Physik, Göttingen, Germany) at the GPMR, China University of Geosciences, Wuhan, China. A "wire" signal smoothing device is included in this laser ablation system, by which smooth signals are produced even at very low laser repetition rates down to 1 Hz (Hu *et al.*, 2012a). Detailed operating conditions for the laser ablation system and the MC-ICP-MS instrument and analytical method are the same as those described by Hu *et al.* (2012a).

The major limitation to accurate *in situ* zircon Hf isotope determination by LA-MC-ICP-MS is the very large isobaric interference from ^{176}Yb and, to a much lesser extent ^{176}Lu on ^{176}Hf (Woodhead *et al.*, 2004). The under- or over-estimation of the β_{Yb} value would undoubtedly affect the accurate correction of ^{176}Yb and thus the determined $^{176}Hf/^{177}Hf$ ratio. We applied the directly obtained β_{Yb} value from the zircon sample itself in real-time (Liu *et al.*, 2010a). The $^{179}Hf/^{177}Hf$ and $^{173}Yb/^{171}Yb$ ratios were used to calculate the mass bias of Hf (β_{Hf}) and Yb (β_{Yb}), which were normalised to $^{179}Hf/^{177}Hf = 0.7325$ and $^{173}Yb/^{171}Yb = 1.1248$ (Blichert-Toft *et al.*, 1997) using an exponential correction for mass bias. Interference of ^{176}Yb on ^{176}Hf was corrected by measuring the interference-free ^{173}Yb isotope and using $^{176}Yb/^{173}Yb = 0.7876$ (McCulloch *et al.*, 1977) to calculate $^{176}Yb/^{177}Hf$. Similarly, the relatively minor interference of ^{176}Lu on ^{176}Hf was corrected by measuring the intensity of the

interference-free ^{175}Lu isotope and using the recommended $^{176}Lu/^{175}Lu = 0.02656$ (Blichert-Toft *et al.*, 1997) to calculate $^{176}Lu/^{177}Hf$. We used the mass bias of Yb (β_{Yb}) to calculate the mass fractionation of Lu because of their similar physicochemical properties. Off-line selection and integration of analytical signals, and mass bias calibrations were performed using *ICPMSDataCal* (Liu *et al.*, 2010a). The zircon Lu-Hf isotopic data are given in Table S4.

5. Results

The compositional characteristics of intermediate dykes and granites are summarised in the following discussion in relation to the different analytical methods. Results of major and trace element compositions, U-Pb zircon dating, zircon Hf and Sr-Nd isotopic compositions, and previously published data are listed in Supplementary Materials and Supplementary Data. References cited with the geochemical data (Supplementary Data) are listed in the Appendix.

5.1 U-Pb zircon geochronology

Three samples of intermediate dykes and nine granites were selected for U-Pb zircon dating; U-Pb age data and Concordia diagrams are presented respectively in Table S1 and Figure 4. Analysed zircon grains are characterized by euhedral and elongate crystals that show significant oscillatory growth zoning in CL images, and by Th/U ratios ranging from 0.21 to 3.38, which imply a magmatic origin (Hoskin and Schaltegger, 2003).

5.1.1 Zhangban Pluton

Zircon grains from five samples of the Zhangban pluton, including biotite-bearing granite (QZ01, 07), monzogranite (QZ11) and intermediate dykes (QZ12, 14), were dated by LA-ICP-MS. Twenty-four spots selected for zircon grains from sample QZ01 produced ages ranging from 104.8 Ma to 100.3 Ma. Excluding six analyses which are discordant or of high

error, the analyses give a weighted mean $^{206}Pb/^{238}U$ age of 102.3 ± 0.8 Ma (Fig. 4a). Eighteen spots from sample QZ07 were analysed, with 10givinga weighted mean $^{206}Pb/^{238}U$ age of 92.1 ± 1.0 Ma (Fig. 4b). Eighteen spots were determined for zircon grains from sample QZ11, of which13give a weighted mean $^{206}Pb/^{238}U$ age of 87.1 ± 0.9 Ma (Fig. 4c). Eighteen spots selected for zircon grains from the intermediate dyke samples (QZ12, 14) were analysed and give weighted mean $^{206}Pb/^{238}U$ ages of 86.9 ± 0.9 Ma and 83.5 ± 0.9 Ma (Fig. 4d, e); rejected analyses are discordant or have high error.

5.1.2 Huian Pluton

For the Huian Pluton, only two monzogranite samples (QZ17, 22) were used for U-Pb LA-ICP-MS zircon dating. Eighteen zircon grains from sample QZ17 were analysed, with ten giving concordant ages from 108.7 Ma to 107.7 Ma and a weighted mean $^{206}Pb/^{238}U$ age of 108.4 ± 0.9 Ma (Fig. 4f). Eighteen zircon grains from sample QZ22 were analysed, with 11 concordant analyses giving a weighted mean $^{206}Pb/^{238}U$ age of 117.6 ± 1.5 Ma (Fig. 4g).

5.1.3 Sidu Pluton

Two monzogranite samples (QZ25, 55) from Sidu Pluton were selected for U-Pb LA-ICP-MS zircon dating. Fourteen zircon grains from sample QZ25 give a weighted mean $^{206}Pb/^{238}U$ age of 133.1 ± 1.3 Ma, with four analyses being discordant (Fig. 4h). Fifteen zircon grains of out of 18 selected from sample QZ55 give a weighted mean $^{206}Pb/^{238}U$ age of 91.4 ± 1.0 Ma, with the other three analyses being discordant (Fig. 4i).

5.1.4 Damaoshan Pluton

We selected only one monzogranite (QZ62) for dating from Damaoshan Pluton. Ten zircon analyses gave a weighted mean $^{206}Pb/^{238}U$ age of 111.3 ± 1.2 Ma (Fig. 4j), another three analyses were excluded because they are discordant, whereas the other five analyses gave older ages ranging from 144.7 Ma to125.7 Ma, which we interpret to be of inherited origin.

The weighted mean $^{206}Pb/^{238}U$ age of 111.3 ± 1.2 Ma is interpreted to be the crystallisation age of the Damaoshan monzogranite.

5.1.5 Xiamen Pluton

One monzogranite sample (XM07) and one intermediate dyke sample (XM08) were chosen for dating of the Xiamen Pluton. Fifteen spots selected from sample XM07 were analysed, giving a weighted mean $^{206}Pb/^{238}U$ age of 114.8 ± 1.8 Ma from 14concordant analyses (Fig. 4k). Although 14 zircon grains were analysed from sample XM08, giving a weighted mean $^{206}Pb/^{238}U$ age of 90.7 ± 1.7 Ma (Fig. 4l), only one analysis is concordant. Discordance between$^{207}Pb/^{235}U$ and$^{207}Pb/^{235}U$ ratios in the analyses is derived from lower ^{207}Pb isotope contents, thereby causing the ICP-MS to give imprecise $^{207}Pb/^{235}U$ ratios. Despite the discordant set of analyses, the mean$^{206}Pb/^{238}U$ age is interpreted to record the crystallisation age of this intermediate dyke.

5.2 Major and trace element geochemistry

Geochemical analyses of 33 samples (see Table S2) combined with previously published data (see Supplementary Data) document the regional scale geochemical characteristics of the coastal Fujian Province.

The plutonic total alkali-silica diagram (Fig. 5a) emphasizes the considerable variations of alkalis versus silica of the five plutons, and serves as a basis for nomenclature (Middlemost, 1994). The intermediate dykes sampled in this study show diverse geochemical compositions, with SiO_2 ranging from 55.1% to 64.4%. One sample of gabbroic diorite (QZ63, $Mg^{\#} = 56$) plots in the monzodiorite field owing to its high LOI value (4.3%), which is compatible with the presence of calcite amygdales seen in thin-section (Fig. 3c). Similarly, quartz and plagioclase phenocrysts (Fig. 3a) in the other two dioritic dyke samples (QZ12, 14) result in

the sample plotting in the granodiorite field. Most of sampled intermediate dykes are medium-K to high-K calc-alkaline rocks (Fig. 5b), and are metaluminous with A/CNK ratios (molar ratio $Al_2O_3/[CaO + K_2O + Na_2O]$) ranging from 0.65 to 1.09 (Fig. 5c).

The majority of granites sampled in this study are characterised by a high range in SiO_2 from 70.2% to 78.8% and in K_2O from 3.1% to 5.3%, indicating that they are high-K calc-alkaline rocks (Fig. 5a, b), but they have low abundances in TiO_2, $Fe_2O_3^T$, MnO, MgO, CaO and P_2O_5. The abundance of Al_2O_3 ranges from 12.2%to 14.9%. Excluding QZ07, the range in A/CNK index from 0.97 to 1.09 establishes that these rocks are metaluminous (Fig. 5c).

Chondrite-normalised rare-earth elements (REEs) and primitive mantle normalised trace-element patterns are shown in Fig. 6. The former invariably show light rare-earth element (LREEs) enrichment and insignificant negative europium anomalies ($Eu/Eu^* = 0.85$ to 0.95) for all intermediate dyke rocks (Fig. 6a). In the primitive mantle normalized variation diagram (Fig. 6b), all intermediate dyke rocks show characteristic negative anomalies in Th, Nb, Ta, and Ti, and positive anomalies for U, Pb, Sr, Zr and Hf. Samples QZ12 and QZ14 have lower abundances in REEs and trace elements, and higher Sr/Y ratios (100 and 89, Fig. 8) than the other samples, which will be explained in the following discussion.

The granites (group 1) on Figure 6c are enriched in LREEs relative to HREEs, with small to moderate negative europium anomalies ($Eu/Eu^* = 0.49$ to 0.85) and flat HREEs patterns. The primitive mantle normalised variation diagram (Fig. 6d) shows that the granites are enriched in large ion lithophile elements (LILEs, such as Rb, Ba, Th, U, K, Pb) and depleted in high field strength elements (HFSEs, such as Nb, Ta, P, Ti).

The fine-grained granites (group 2) are enriched in LREEs relative to HREEs with significant negative europium anomalies ($Eu/Eu^* = 0.17$ to 0.49, except for QZ19) and inverse

HREEs patterns (except for QZ05) (Fig. 6e). On a primitive mantle normalised variation diagram (Fig. 6f), all the fine-grained granites are enriched in LILEs (Rb, Ba, Sr, Th, U, K, Pb) and seriously depleted in HFSEs (Nb, Ta, P, Ti).

5.3 Sr-Nd isotopic geochemistry

Bulk-rock Sr-Nd isotopic compositions of representative samples from QZ and XM are listed in Table S3 and plotted on Fig. 7a, b. Initial $^{87}Sr/^{86}Sr$ ratios, and $\varepsilon_{Nd}(t)$ values have been calculated using ages obtained in this study. All the granites have initial $^{87}Sr/^{86}Sr$ ratios of 0.704817 to 0.706108 and $\varepsilon_{Nd}(t)$ values of -1.2 to -4.4, with Nd model ages ranging from 0.87 Ga to 1.20 Ga. The intermediate dykes have similar Sr-Nd isotopic compositions ($^{87}Sr/^{86}Sr_i$ = 0.705659 to 0.706223; $\varepsilon_{Nd}(t)$ = -1.2 to -2.7), with Nd model ages ranging from 0.92 Ga to 1.14 Ga.

5.4 Zircon Hf isotope geochemistry

In situ Hf isotopic data of zircon grains from six granite samples and two intermediate dyke samples are listed in Table S4, and shown alongside previously published data in Fig. 7c. In situ zircon U-Pb ages were used to calculate $\varepsilon_{Hf}(t)$ values and Hf model ages. Two intermediate dykes (QZ12 and XM08) show positive $\varepsilon_{Hf}(t)$ values ranging from +2.7 to +7.6, corresponding to Cambrian-Neoproterozoic Hf mantle model ages (T_{DM}) of 0.48 Ga to 0.67 Ga. Granites also gave positive $\varepsilon_{Hf}(t)$ values (-0.5 to +9.9), except for the $\varepsilon_{Hf}(t)$ values of sample QZ25 (-2.8 to +1.0), corresponding to Neoproterozoic-Mesoproterozoic Hf crust model ages of 0.54 Ga to 1.37 Ga. On the basis of published data, it appears that a mantle contribution to granites increased with decreasing zircon U-Pb ages. This spatial-temporal evolution is explained below.

6. Discussion

6.1 Temporal and spatial distribution of Cretaceous magmatism in Fujian Province

As Figure 1shows, most Middle-Late Jurassic igneous rocks are located within the Cathaysia Block whereas the great majority of Cretaceous igneous rocks are distributed along the coastal belt. In particular, there are vast areas of Cretaceous granites in coastal Fujian Province.

We have reviewed most of the published age-data (see Supplementary Data) on the Cretaceous granites and associated basic-intermediate dykes. Generally, inland granites are older than coastal granites (Fig. 1), although magmatic stages can be preserved in the same pluton along the coastal belt (Fig. 8a). This is particularly significant in Quanzhou and Xiamen (Fig. 2a, b). We suggest that the migration of granite magmatism from inland to coastal regions was the result of subduction retreat from the late Jurassic to the late Cretaceous. The age data indicate that the principal stage of granite magmatism occurred from 120 Ma to 90 Ma (Fig. 8b), and that basic-intermediate magmatism in these granites occurred between 120 Ma to 80 Ma (Fig. 8c). This implies that mantle-derived magmas contributed significantly to the crust over the peak magmatic period (i.e., 120 Ma to 80 Ma).

Five Cretaceous A-type granite plutons are exposed along the sinistral Changle-Nan'ao Fault Zone (CNF). Although the genesis of A-type granite is controversial, there is consensus that A-type granites relate to shallow level high-temperature and low-pressure conditions of the middle to upper crust, as determined by experimental petrology (Clemens *et al.*, 1986; Patiño Douce, 1997). Coupled with a mantle contribution between 120 Ma to 80 Ma, the implication is that the Cretaceous tectonic setting of coastal Fujian Province was extensional.

6.2 Magmatic sources and petrogenesis

6.2.1 Granites

6.2.1.1 Sources of granite magmas

The subdivision of I-type (igneous source) and S-type (sedimentary source) granites was proposed by Chappell and White (1974), and subsequently applied world-wide. Granites studied here are characterised by high K_2O (to 5.3%), low FeO*/MgO ratios (2.6 to 6.7) (Fig. 9a) and A/CNK values (<1.1) (Fig. 5c), and mostly fall in the high-K calc-alkaline series (Fig. 5b). In addition, P_2O_5 decreases (<0.1%) with increasing SiO_2, because apatite attains saturation in metaluminous and slightly peraluminous magmas but has high solubility in strongly peraluminous melts (Wolf and London, 1994) (Fig. 9b). Yttrium and Th increase as Rb increases (Fig. 9c, d), thereby showing a typical I-type granite evolution trend (Eby, 1990; Chappell, 1999). Combined with field geology (Fig. 2a, b), we suggest that the widespread dynamic-metamorphic rocks (T-J) were at least a small portion of the source for the granites in this study. Consequently, the granites are typical high-K calc-alkaline I-type granites. Group 2 granites have significant negative anomalies of Eu, Ba, Sr, P and Ti on spidergrams (Fig. 6e, f), suggesting that the granites are highly fractionated I-types (Wu *et al.*, 2003).

Although granites in Quanzhou and Xiamen have four classifications based on their petrography, they are collectively characterised by low initial $^{87}Sr/^{86}Sr$ ratios, slightly negative $\varepsilon_{Nd}(t)$ values (Table S3) and positive $\varepsilon_{Hf}(t)$ values (Table S4), with the exception of sample QZ25. Low initial $^{87}Sr/^{86}Sr$ ratios (0.705 to 0.706) and slightly negative $\varepsilon_{Nd}(t)$ values (-1.2 to -4.4) (Fig. 7a) with young Nd model ages (0.87 to 1.20 Ga) indicate that the mantle contributed to the formation of the granites, or that the granites were mainly derived from the melting of juvenile crust. Positive $\varepsilon_{Hf}(t)$ values (-0.5 to 9.9) (Fig. 7b) and young Hf crust model ages (0.54 to 1.21 Ga) establish that the granites were mainly derived from the partial

melting of juvenile crustal sources. Sample QZ25 has more negative ε_{Nd} (t) and lower negative ε_{Hf} (t) values than the other granites, indicating that its source had a more ancient crustal composition.

6.2.1.2 Petrogenesis of granites

Published work in recent years has shown that granitic magmas can be formed in an extensional setting. In particular, granites in subduction-related settings are associated with the extension of the continental lithosphere and its underplating by basaltic magmas derived from the mantle (Chen *et al.*, 2014; Li *et al.*, 2014; Qiu *et al.*, 2012; Wang and Shu, 2012; Zhou *et al.*, 2006; Zhou and Li, 2000). As mentioned above, the relatively high ε_{Nd} (t) values (-1.2 to -2.7), young Nd model ages (0.87 Ga to 1.20 Ga) and positive ε_{Hf} (t) values (-0.5 to 9.9) of the granites, excluding sample QZ25, indicate that the granites contain a significant mantle component. The Nd-Hf isotopic compositions of the granites are homogeneous and this (Table S3, S4 and Fig. 7a, b), further demonstrates that the granites were derived from the melting of juvenile crust (Bolhar *et al.*, 2008). Sample QZ25 has low ε_{Nd} (t) values (-4.4) and intermediate ε_{Hf} (t) values (1.0 to -2.8), suggesting that the granite crystallised from magma formed by mixing between crustal and mantle end-members (Fig. 7a, b).

Cumulate basic granulite xenoliths (CBGX, with a Sr-Nd isochron age of 115 Ma) from Qilin (Fig. 1) have the characteristics of depleted mantle (Fig. 7a), namely low K_2O (0.04% to 0.34%) and P_2O_5 (0.02% to 0.04%), and high CaO (9.9% to 14.7%). However, magmatic basic granulite xenoliths (MBGX) have similar Sr-Nd isotopic compositions (i.e., juvenile) to the granites, namely high K_2O (0.5% to 1.6%) and P_2O_5 (0.3% to 0.7%), and low CaO (6.6% to 8.7%) (Yu *et al.*, 2003); in particular, REE patterns are similar to the granites. We suggest that fractional crystallization of a magma, with a source mixed between underplated basalt and

lower crust, produced the magmatic basic granulite layer, above which amphibolite remains and makes up the composition of the middle-crust or the upper lower-crust (Fig. 11a). Consequently, we consider that the granites were formed from magmas that melted amphibolite, and assimilated country rocks during their emplacement in shallow-level chambers.

The $\varepsilon_{Hf}(t)$ values of the granites have an obvious linear trend, increasing with granite age, which become younger from inland to the coast (Fig. 7b). The Hf isotopic composition of zircon grains in granites records ages earlier than Sr-Nd isotopic compositions due to the high closure temperature of zircon. In addition, zircon Hf crustal model ages of the granites and the zircon Hf mantle model ages of the dykes imply there was a common mantle contribution to the crust between 120 Ma and 90 Ma, particularly in the granites which show an increasing trend during that period (Fig. 7c, d). Therefore, we suggest that the contribution from the mantle increased from 133 Ma to 84 Ma. Considering the origin of the I-type granites studied here, it appears that an extensional setting for coastal Fujian Province played a crucial role in lithospheric evolution during Mesozoic subduction of the Palaeo-Pacific slab. This is supported by the results from the Sinoprobe02-04 Project, whose conductivity characteristics of the magnetotelluric profile in the coastal area of southeastern China show thinned lithosphere and upwelling asthenosphere (Liu *et al*., 2012).

6.2.2Dykes

6.2.2.1 The cross-cutting relationship between host rocks and dykes

The co-existence of basic-intermediate and felsic magmas appears compelling based on our field observations (Fig. 2c, d). The dykes have sharp, chilled contacts with their host granites and a gradational mixed magma zone is poorly defined. These relationships indicate that the host granites had a crystal content greater than 80% before the intermediate magmas

were injected along fractures to form continuous dykes, as explained by the four-stage model proposed by Barbarin and Didier (1992) and Barbarin (2005). This indicates that mixing between granite and dyke magmas did not occur. Furthermore, petrographic observations suggest that quartz and plagioclase xenocrysts did not crystallise from dyke magmas because of their resorbed margins (Fig. 3a), whereas our dating shows that the emplacement of dyke magmas (90 Ma to 84 Ma) slightly post-dates emplacement of the host granites (115 to 87 Ma). However, samples QZ11 and QZ12 have similar ages (~ 87 Ma). Based on outcrop features of chilled margins with angular and flat joint surfaces that were created by plastic flow during cooling, we suggest that sample QZ12 is of a synplutonic dyke that invaded an unconsolidated, yet relatively cooler granitic host (QZ11) (Figure S1). Furthermore, because zircon U-Pb ages have errors of between 1 and 2 million years, it is reasonable assume that the dyke and host granite have similar ages. Because of the relatively small volume of dyke magma, cooling was probably so rapid that there was limited opportunity for chemical interaction between the two magmas (cf. Wiebe, 1991). Consequently, the dykes have no genetic link to the granites and magma mixing was negligible.

6.2.2.2Petrogenesisof dykes

Fractional crystallization within cooling basaltic magmas can generate mafic crystals and anorthites, which then accumulate in the lower part of the magma chamber (Bowen, 1922). The residual melt gradually enriches in silica and incompatible elements, such as K, Rb, Ba, U, Pb. Harker diagrams of selected major elements from the dyke samples show that the weight percentages of Na_2O and Al_2O_3 increase with silica content (Fig. 10a, b), whereas the opposite occurs with CaO and MgO (Fig. 10c, d). These data therefore appear to conform to a fractional crystallization model. The decreasing content of K_2O with decreasing silica content,

however, is not the result of the fractional crystallization model (Fig. 5b), even if the values of all regional basic-intermediate dykes or plutons have increasing silica content. Therefore, the petrogenesis of the dykes cannot completely be explained by the fractional crystallization of a basalt magma derived from the melting of lithospheric mantle.

The intermediate~90 Ma dykes from Xiamen have low MgO (2.9% to 4.2%), Ni (31 ppm to 72 ppm) and Cr (40 ppm to 96 ppm) and low SiO_2 (55% to 58%), Al_2O_3 (16.8% to 17.2%) contents (Table S2), suggesting that their parental magmas were unlikely to have been directly derived from mantle sources. Their negative $\varepsilon_{Nd}(t)$ values and positive $\varepsilon_{Hf}(t)$ values suggest that their parental melts were not derived from enriched mantle but formed by mixing of mantle-derived basaltic magma and crustal-derived melt (Fig. 7a, b). This is shown by high Nb/Ta ratios (17 to 20) and Th/Yb ratios (1.4 to 2.5), similar to the middle-lower crust, and by the Fe-Mg diagram (Fig. 11a, b, c). As described above, magmatic basic granulite xenoliths (MBGX)from Qilin have similar Sr-Nd isotopic compositions, enriched LILEs (Rb, Ba, U, K, Pb, Sr), OIB-like rare earth elements, and depleted HFSEs (Nb, Ta, Ti) like the dykes (Fig. 6a, b). Therefore, it appears that the Xiamen dykes were derived from residual basic lower crust after mafic crystal accumulation.

In addition, the dykes from Quanzhou, excluding samples QZ12 and QZ14, have similar geochemical characteristics to the Xiamen dykes, particularly samples QZ02 and QZ63. Nevertheless, the other samples have relative low Th/Yb ratios and high Nb/Yb ratios (Fig. 11 b). Considering the geochemical similarity Xiamen dykes, we suggest that the Quanzhou dykes are products of the late melting stage of the same sources.

Samples QZ12 and QZ14 are characterised by high Sr/Y ratios, which are typical features of adakitic rocks (Fig. 11d). Adakites are defined by Defant and Drummond (1990) as rocks

resulting from the partial melting of a subducted slab in the garnet stability field. Recent studies have shown that adakitic rocks can form by the partial melting of recently underplated or thickened crust (Atherton and Petford, 1993; Chung *et al.*, 2003; Condie, 2005; Sheppard *et al.*, 2001; Wang *et al.*, 2005), fractionation of mantle-derived primitive arc magma (Castillo *et al.*, 1999; Macpherson *et al.*, 2006; Richards and Kerrich, 2007; Roderíguez *et al.*, 2007), and mixing between mantle- and crust-derived melts (Danyushevsky *et al.*, 2008; Xu *et al.*, 2012).The high Sr/Y ratios (89 to 100) and high SiO_2 (63.12%),low K_2O (1.5% to 1.6%), Ni (15 ppm to 16 ppm) and Cr (~20 ppm) contents of the adakitic samples indicate that the rocks were unlikely to have been derived from thickened crust (Moyen, 2009; Wang *et al.*, 2005) or the fractionation of mantle-derived primitive arc magma. In combination with their slightly negative ε_{Nd} (t) values (-1.7 to -1.8) and positive ε_{Hf} (t) values (2.9 to 4.3), we suggest that the adakitic rocks were derived from a mixed lower crust source, between depleted mantle- and crust-derived melts. The high content of Sr may derive from melting of plagioclase in the cumulate basic granulite xenoliths (CBGX), which have the features of depleted mantle (Yu *et al.*, 2003).

6.3 Brief review on Cretaceous adakite-like rocks in coastal Fujian Province

Previously published work on Mesozoic granites and basic-intermediate dykes/plutons of coastal Fujian Province has documented some adakite-like rocks (see the samples identified by asterisks on the trace element sheets in Supplementary Data and on Fig. 11d), comprising several basic-intermediate dykes/plutons and 12 granites. It appears that those granites or basic-intermediate dykes/plutons crystallised between 110 Ma and 90 Ma. The granites have been proposed to be derived from a mixed source comprising depleted mantle and crustal

components (Fig. 7a, b; Li *et al.*, 2012b; Qiu *et al.*, 2012; Zhao *et al.*, 2012). With regards to the petrogenesis of gabbroic plutons, Chen *et al.* (2004) suggested high Sr/Y gabbros formed from the dehydration melting of amphibolite, whereas the gabbros from Quanzhou and Tong'an were interpreted to have originated from mantle-derived magmas contaminated by a crustal component (Li *et al.*, 2012a; Zhou and Chen, 2001). In contrast, Zhao (2004b) advocated that the Putian gabbroic intrusion had not experienced much crustal assimilation but rather metasomatism before its emplacement. Finally, high Sr/Y basic-intermediate dykes from Tuling and Meizhoudao were interpreted to be the products of mixed contributions from Palaeo-Pacific slab subduction and crust-mantle interaction (Dong *et al.*, 2011; Yang *et al.*, 2010a; Zhao, 2004b). Although those authors derived different petrogenetic models from their geochemical results, Cretaceous lithospheric extension and subduction of the Palaeo-Pacific slab were emphasised.

6.4 Implications for Cretaceous lithospheric evolution

6.4.1 Cretaceous extensional setting

As discussed above, previously published work has suggested that granite can be formed in an extensional setting. In particular, granites emplaced in a subduction-related tectonic setting are associated with the extension of the overlying continental lithosphere and the underplating of basaltic magmas derived from the mantle (Chen *et al.*, 2014; He and Xu, 2012; Li *et al.*, 2014; Qiu *et al.*, 2012; Wang and Shu, 2012; Yang *et al.*, 2013; Zhou *et al.*, 2006; Zhou and Li, 2000). The 105 Ma to 90 Ma A-type granites along the Changle-Nan'ao Fault Zone in the coastal Fujian Province (Fig. 8a) imply, based on petrology and experimental petrology (e.g., Clemens *et al.*, 1986; Patiño Douce, 1997), a high temperature, low pressure tectonic environment. In addition, comprehensive geochronological studies (by K-Ar and

$^{40}Ar/^{39}Ar$methods) of basic dykes and plutons in Fujian Province (Zhao, 2004b) and in Guangdong Province (Li and McCulloch, 1998) divide the basic magmatism into five stages, namely: 140 Ma to 135 Ma, 125 Ma, 110 Ma to 105 Ma, 90 Ma to 85 Ma and 75 Ma to 70 Ma. Furthermore, SHRIMP U-Pb zircon ages of basic dykes from Jinjiang, Tong' an and Meizhoudao in the coastal Fujian Province range from 96 Ma to 87 Ma (Dong *et al.*, 2006, 2011; Yang *et al.*, 2010b). These studies suggest that an extensional setting dominated Cretaceous magmatic-tectonic interaction in the coastal belt, which can also be linked to the Changle-Nan'ao Fault Zone (Shi and Zhang, 2010; Wang and Lu, 1997, 2000). In conjunction with the results of our work, we suggest that extension-induced middle-lower crustal melting and underplating by mantle-derived basaltic melts were the principal driving mechanisms for Cretaceous granitic magmatism in coastal Fujian Province. Figure 12 is a schematic view of the tectonomagmatic scenario for the 120 Ma to 80 Ma magmatic stage. The later part of that stage may be related to sinistral strike-slip along the Changle-Nan'ao Fault Zone from 112 Ma to 95 Ma (Wang *et al.*, 2013).

6.4.2 Cretaceous continental crust growth

Crustal growth is the process by which rocks of a depleted mantle composition are added to continental crust (Wu *et al.*, 2007). Cretaceous granites in coastal Fujian Province comprise mainly I- and A-type (Chen *et al.*, 2013, 2014; Li *et al.*, 2012b; Qiu *et al.*, 1999, 2000, 2012); whereas S-type granites are absent. All the granites studied here are I-type. Their isotopic geochemical characteristics imply a depleted mantle contribution to Cretaceous continental crust of the southeastern Cathaysia Plate. This study, in combination with previously published work, suggests that the period of depleted mantle contribution to the continental crust occurred between 120 Ma to 80 Ma. Growth of continental crust is

inherently related to subduction-related processes, such that active continental margins are generally considered to be the principal sites for the formation of continental crust (Ernst, 2000; Middlemost, 1997; Oncken *et al.*, 2006). The Cretaceous tectonic setting of the southeastern Cathaysia Plate was an active continental margin, thereby explaining why there was intense magmatic activity of the mantle between 120 Ma to 80 Ma, as indicated by the isotope geochemistry reported here. Consequently, we consider that underplating basalt magmatism is the important mechanism for continental crust growth at subduction zones. Continental crust growth continued into the Cainozoic, for example during the formation of the Philippine Sea Plate (Yin, 2010). Crustal growth of the southeastern Cathaysia Plate was much younger than the 200 Ma to 150 Ma crustal growth of northeastern China (Wu *et al.*, 2000), and this age difference relates to a different period of Palaeo-Pacific slab subduction.

6.4.3 Geodynamics of palaeo-Pacific slab subduction

Lithospheric growth associated with oceanic plate subduction under continental margins is triggered by dehydration of the sinking slab, so that regions surrounding the Pacific Ocean are a natural laboratory for lithospheric research. The Pacific slab under southeastern China is shown to be stagnant in the mantle transition zone on tomographic imagery (Huang and Zhao, 2006). Some studies consider that the transition-zone slab of the Palaeo-Pacific Plate beneath eastern China resulted from westward flat-subduction during the Mesozoic (e.g., Li and Li, 2007; Li *et al.*, 2007; Meng *et al.*, 2012). This model is unrealistic due to the lack of a driving force for flat-subduction and it is more likely that the slab was left behind as the result of western Pacific subduction retreat (Fig. 12) under gravity (Niu, 2014).

Since the beginning of the early Cretaceous (145 Ma), the dip angle of the subducting slab has increased (Zhou and Li, 2000). Fast subduction gave rise to incomplete dehydration

and oceanic crust eclogitization was not exhaustive. During the late stage of the early Cretaceous and the early stage of the late Cretaceous (120 Ma to 80 Ma), the low density of the subducted slab mean that the slab could not sink into the lower mantle. Stable gravity in the mantle transition zone made the dip angle of subducted slab increase further, the response to which, at the crustal level, was trench retreat (Niu, 2014), which resulted in lithospheric extension.

However, if a subducting slab quickly reaches thermal equilibrium and thus passes below 660 km depth and enters the lower mantle, subduction retreat is slowed (Li *et al.*, 2008). In contrast, the Palaeo-Pacific slab in the transition zone confirms a fast speed of subduction which produced a stagnant slab in the mantle transition zone. This interpretation is supported by a period (109 Ma to 90 Ma) of rapid subduction beneath southeastern China (Jahn, 1974). The temporal and spatial distribution of Cretaceous magmatism in Fujian Province, as discussed above, establishes a significant subduction retreat from inland to offshore as do the $\varepsilon_{Hf}(t)$ values. Hence, we conclude that fast trench/subduction retreat, which resulted in the extensional setting, and steep slab subduction, which resulted in the underplating of mantle-derived basaltic melts, were coupled and mainly responsible for the Cretaceous tectonic transition from compression to extension in the coastal belt of southeastern China.

7. Conclusions

Main findings of the present study are summarised as follows.

1) The ages of granites and intermediate dykes range respectively from 133 Ma to 87 Ma and from 90 Ma to 84 Ma. Inland granitic magmatism is older than coastal granitic magmatism. The dykes do not have a genetic link with the granites, and magma mixing was negligible.

2) Similar elemental and isotopic geochemical characteristics of the granites indicate the granites were produced by the ascent of magma that melted from amphibolite in the middle-lower crust, and which may have assimilated country rocks during emplacement in a shallow chamber. Adakite-like dykes were derived from a source mixed between depleted mantle-derived and crust-derived melts. The high content of Sr originated from the melting of plagioclase in cumulate basic granulite xenoliths (CBGX), which have the features of depleted mantle. Other dykes were derived from residual basic lower crust after mafic crystals accumulation.

3) Extension-induced middle-lower crustal melting and underplating of mantle-derived basaltic melts are suggested as the principal driving mechanisms for Cretaceous granitic magmatism in coastal Fujian Province. The period of continental crust growth in the coastal Cathaysia Plate was between 120 Ma to 80 Ma, which is later than crustal growth (200 Ma to 150 Ma) recorded in northeastern China, and may have continued into the Cainozoic.

4) Fast subduction retreat produced the extensional setting, and the accompanying steep slab subduction caused underplating of mantle-derived basaltic melts. These tectonic processes were coupled and mainly responsible for the Cretaceous tectonic transition from compression to extension in the coastal belt of the Cathaysia Plate.

Acknowledgements

We thank editor Andrew Kerr, for handling this manuscript and two anonymous reviewers for constructive comments. We are grateful to Zhaochu Hu and Yongsheng Liu for guidance on zircon U–Pb dating, Hf isotope, and bulk-rock trace element analyses. We thank Hong Qinfor her help during major elementanalysis. We also thank Yu Huang, Wenxia Li, Fanyi Meng and Yue Chen for their help during Sr-Nd isotope analyses. Bryan Krapež is thanked for help with English writing. This study was supported by Program SINOPROBE-04-02, the Special Funds for Sciences and Technology Research of Public Welfare Trades (No. 201011054), Guangxi National Natural Science Foundation of China (No. 2016GXNSFBA380070), and the research grant of Guangxi Key Laboratory of Hidden Metallic Ore Deposits Exploration (No. 15-140-27-13).

References

Andersen, T., 2002. Correction of common lead in U-Pb analyses that do not report ^{204}Pb. Chemical Geology 192, 59-79.

Annen, C., Sparks, R. S. J., 2002. Effects of repetitive emplacement of basaltic intrusions on thermal evolution and melt generation in the crust. Earth and Planetary Science Letters 203, 937-955.

Atherton, M.P., Petford, N., 1993. Generation of sodium-rich magmas from newly underplated basaltic crust. Nature 362, 144–146.

Barbarin, B., 2005. Mafic magmatic enclaves and mafic rocks associated with some granitoids of the central Sierra Nevada batholith, California: nature, origin, and relations with the hosts. Lithos80, 155-177.

Barbarin, B., Didier, J., 1992. Genesis and evolution of mafic microgranular enclaves through various types of interaction between coexisting felsic and mafic magmas. Transactions of the Royal Society of Edinburgh: Earth Sciences83, 145-153.

Bergantz, G.W., 1989. Underplating and Partial Melting: Implications for Melt Generation and Extraction. Science 245, 1093-1095.

Blichert-Toft, J., Chauvel, C., Albarède, F., 1997. Separation of Hf and Lu for high-precision isotope analysis of rock samples by magnetic sector-multiple collector ICP-MS. Contributions to Mineralogy and Petrology 127, 248-260.

Bolhar, R., Weaver, S.D., Whitehouse, M.J., Palin, J.M., Woodhead, J.D., Cole, J.W., 2008. Sources and evolution of arc magmas inferred from coupled O and Hf isotope systematics of plutonic zircons from the Cretaceous Separation Point Suite (New Zealand). Earth and Planetary Science Letters 268, 312-324.

Bowen, N.L., 1922. The reaction principle in petrogenesis. Journal of Geology 30, 177-198.

Castillo, P.R., Janney, P.E., Solidum, R.U., 1999. Petrology and geochemistry of Camiguin Island, southern Philippines: insights to the source of adakites and other lavas in a complex arc setting. Contributions to Mineralogy and Petrology 134, 33–51.

Chappell, B.W., White, A.J.R., 1974. Two contrasting granite types. Pacific Geology 8, 173-174.

Chappell, B.W., 1999. Aluminium saturation in I- and S-type granites and the characterization of fractionated haplogranites. Lithos 46, 535-551.

Charvet, J., Lapierre, H., Yu, Y.W., 1994. Geodynamic significance of the Mesozoic volcanism of southeastern China. Journal of Southeast Asian Earth Sciences 9 (4), 387-396.

Chen, C.H., Lin, W., Lan, C.Y., Lee, C.Y., 2004. Geochemical, Sr and Nd isotopic characteristics and tectonic implications for three stages of igneous rock in the Late Yanshanian (Cretaceous) orogeny, SE China. Transactions of the Royal Society of Edinburgh: Earth Sciences 95, 237-248.

Chen, J.Y., Yang, J.H., Zhang, J.H., Sun, J.F., Wilde, S.A., 2013. Petrogenesis of the Cretaceous Zhangzhou batholith in southeastern China: Zircon U-Pb age and Sr-Nd-Hf-O isotopic evidence. Lithos 162-163, 140-156.

Chen, J.Y., Yang, J.H., Zhang, J.H., Sun, J.F., 2014. Geochemical transition shown by Cretaceous granitoids in southeastern China: Implications for continental crustal reworking and growth. Lithos 196-197, 115-130.

Chen, W., Yang, H., Wang, X., Huang, H., 2002. Tectonic setting and exhumation history of the Pingtan-Dongshan metamorphic belt along the coastal sea, Fujian Province, Southeast China. Journal of Asia Earth Sciences 20, 829-840.

Chung, S.L., Liu, D.Y., Ji, J.Q., Chu, M.F., Lee, H.Y., Wen, D.J., Lo, C.H., Lee, T.Y., Qian, Q., Zhang, Q.,

2003. Adakites from continental collision zones: melting of thickened lower crust beneath southern Tibet. Geology 31, 1021–1024.

Clements, J.D., Holloway, J.R., White, A.J.R., 1986. Origin of an A-type granite: experimental constraints. American Mineralogist71, 317-324.

Condie, K.C., 2005. TTGs and adakites: are they both slab melts? Lithos 80, 33–44.

Danyushevsky, L.V., Falloon, T.J., Crawford, A.J., Tetroeva, S.A., Leslie, R.L., Verbeeten, A., 2008. High-Mg adakites from Kadavu Island Group, Fiji, southwest Pacific: evidence for the mantle origin of adakite parental melts. Geology 36, 499-502.

Defant, M.J., Drummond, M.S., 1990. Derivation of some modern arc magmas by melting of young subducted lithosphere. Nature 347, 662-665.

Dong, C.W., Zhang, D.R., Xu, X.S., Yan, Q., Zhu, G.Q., 2006. SHRIMP U-Pb dating and lithogeochemistry of basic-intermediate dyke swarms from Jinjiang, Fujian Province. Acta Petrologica Sinica 22 (6), 1696-1702 (in Chinese with English abstract).

Dong, C.W., Zhou, C., Gu, H.Y., Ma, X.X., Lü, Q., 2011. The Age Difference, Geochemistry and Petrogenesis of Mafic Dykes and Host Granites from Meizhou Island in Fujian Province. Journal of Jilin University (Earth Science Edition) 41 (3), 735-744 (in Chinese with English abstract).

Eby, G.N., 1990. The A-type granitoids: A review of their occurrence and chemical characteristics and speculations on their petrogenesis. In: Woolley, A.R., Ross, M. (Editors), alkaline igneous rocks and carbonatites. Lithos 26, 115-134.

Ernst, W.G., 2000. Earth systems: processes and issues. Cambridge University Press, pp 576.

Foley, S.F., Tiepolo, M., Vannucci, R., 2002. Growth of early continental crust controlled by melting of amphibolite in subduction zones. Nature 417, 637-640.

FJBGMR (Fujian Bureau of Geology and Mineral Resource), 1985. Regional Geology of Fujian Province. Geological Publication House, Beijing. 671pp(in Chinese with English summary).

He, Z.Y., Xu, X.S., 2012. Petrogenesis of the Late Yanshanian mantle-derived intrusions in southeastern China: Response to the geodynamics of palaeo-Pacific plate subduction. Chemical Geology 328, 208-2211.

Hoskin, P.W.O., Schaltegger, U., 2003. The composition of zircon and igneous and metamorphic petrogenesis. Reviews in Mineralogy and Geochemistry 53: 27-62.

Hu, Z., Liu, Y., Gao, S., Xiao, S., Zhao, L., Günther, D., Li, M., Zhang, W., Zong, K., 2012a. A "wire" signal smoothing device for laser ablation inductively coupled plasma mass spectrometry analysis. Spectrochimica Acta Part B 78, 50-57.

Hu, Z., Liu, Y., Gao, S., Liu, W., Zhang, W., Tong, X., Lin, L., Zong, K., Li, M., Chen, H., Zhou, L., Yang, L., 2012b. Improved in situ Hf isotope ratio analysis of zircon using newly designed X skimmer cone and Jet sample cone in combination with the addition of nitrogen by laser ablation multiple collector ICP-MS. Journal of Analytical Atomic Spectrometry 27, 1391-1399.

Huang, J., Zhao D., 2006. High-resolution mantle tomography of China and surrounding regions. Journal of Geophysical Research 111, B09305, doi: 10.1029/2005JB004066.

Huang, Z., Wang, L., Zhao, D., Xu, M., Mi, N., Yu, D., Li, H., Li, C., 2010. Upper mantle structure and dynamics beneath Southeast China. Physics of the Earth and Planetary Interiors 182, 161-169.

Huppert, H. E., Sparks, R. S. J., 1988. The generation of granitic magmas by intrusion of basalt into continental crust. Journal of petrology 29, 599-642.

Jahn, B.M., 1974. Mesozoic thermal events in southeast China. Nature 248, 480-483.

Jahn, B.M., Zhou, X.H., Li, J.L., 1990. Formation and tectonic evolution of southeastern China and Taiwan: isotopic and geochemical constraints. Tectonophysics 183, 145-160.

Klimetz, M.P., 1983. Speculations on the Mesozoic plate tectonic evolution of eastern China. Tectonics 2, 139-166.

Li, C., van der Hilst, R., Engdahl, E.R., Burdick, S., 2008. A new global model for P wave speed variation in Earth's mantle. Geochemistry, Geophysics, Geosystem 9: doi:10.1029/2007GC001806.

Li, X.H., Li, Z.X., Li, W.X., Liu, Y., Yuan, C., Wei, G.J., Qi, C.S., 2007. U-Pb zircon, geochemical and Sr-Nd-Hf isotopic constraints on age and origin of Jurassic I- and A-type granites from central Guangdong, SE China: a major igneous event in response to foundering of a subducted flat-slab? Lithos 96, 186-204.

Li, X., McCulloch, M. T., 1998. Geochemical characteristics of cretaceous mafic dikes from Northern Guangdong, SE China: Age, origin and tectonic significance, in Mantle Dynamics and Plate Interactions in East Asia, Geodynamics Series, vol. 27, edited by Flower M. F. J. et al., pp. 405-419, AGU, Washington, D. C., doi:10.1029/GD027p0405.

Li, Z., Qiu, J.S., Xu, X.S., 2012a. Geochronological, geochemical and Sr-Nd-Hf isotopic constraints on petrogenesis of Late Mesozoic gabbro-granite complexes on the southeast coast of Fujian, South China: insights into a depleted mantle source region and crust-mantle interactions. Geological Magazine 149 (3), 459-482.

Li, Z., Qiu, J.S., Zhou, J.C., 2012b. Geochronology, geochemistry, and Nd-Hf isotopes of early Palaeozoic-early Mesozoic I-type granites from the Hufang composite pluton, Fujian, South China: crust-mantle interactions and tectonic implications. International Geology

Review 54, 15-32.

Li, Z., Qiu, J.S., Yang, X.M., 2014. A review of the geochronology and geochemistry of Late Yanshanian (Cretaceous) plutons along the Fujian coastal area of southeastern China: Implications for magma evolution related to slab break-off and rollback in the Cretaceous. Earth-Science Reviews 128, 232-248.

Li, Z.X., Li, X.H., 2007. Formation of the 1300-km-wide intracontinental orogen and postorogenic magmatic province in Mesozoic South China: A flat-slab subduction model. Geology 35, 179-182.

Liu, G.X., Han, K., Han, J.T., 2012. Lithosphere electrical structure in Southeast coastal region, South China. Journal of Jilin University (Earth Science Edition) 42, 536-544 (in Chinese with English abstract).

Liu, Y.S., Gao, S., Hu, Z.C., Gao, C.G., Zong, K.Q., Wang, D.B., 2010a. Continental and oceanic crust recycling-induced melt-peridotite interactions in the Trans-North China Orogen: U-Pb dating, Hf isotopes and trace elements in zircons of mantle xenoliths. Journal of Petrology 51: 537-571.Liu, Y.S., Gao, S., Yuan, H.L., Zhou, L., Liu, X.M., Wang, X.C., Hu, Z.C., Wang, L.S., 2004. U-Pb zircon ages and Nd, Sr, and Pb isotopes of lower crustal xenoliths from North China Craton: insights on evolution of lower continental crust. Chemical Geology 211, 87-109.

Liu, Y.S., Hu, Z.C., Gao, S., Gunther, D., Xu, J., Gao, C.G., Chen, H.H., 2008a. In situ analysis of major and trace elements of anhydrous minerals by LA-ICP-MS without applying an internal standard. Chemical Geology 257, 34-43.

Liu, Y.S., Hu, Z.C., Zong, K.Q., Gao, C.G., Gao, S., Xu, J.A., Chen, H.H., 2010b. Reappraisement and refinement of zircon U-Pb isotope and trace element analyses by LA-ICP-MS. Chinese

Science Bulletin 55, 1535-1546.

Liu, Y.S., Zong, K.Q., Kelemen, P.B., Gao, S., 2008b. Geochemistry and magmatic history of eclogites and ultramafic rocks from the Chinese continental scientific drill hole: Subduction and ultrahigh-pressure metamorphism of lower crustal cumulates. Chemical Geology 247: 133-153.

Ludwig, K.R., 2003. ISOPLOT 3.00: A Geochronological Toolkit for Microsoft Excel. Berkeley Geochronology Center, California, Berkeley (39 pp).

Maniar, P.D., Piccoli, P.M., 1989. Tectonic discrimination of granitoids. Geological Society of America Bulletin 101: 635-643.

Macpherson, C.G., Dreher, S.T., Thirlwall, M.F., 2006. Adakites without slab-melting: high pressure differentiation of island arc magma, Mindanao, the Philippines. Earth and Planetary Science Letters 243, 581–593.

McCulloch, M.T., Rosman, K.J.R., De Laeter, J.R., 1977. The isotopic and elemental abundance of ytterbium in meteorites and terrestrial samples. Geochimica et Cosmochimica Acta 41: 1703-1707.

Meng, L.F., Li, Z.X, Chen, H.L., Li, X.H., Wang, X.C., 2012. Geochronological and geochemical results from Mesozoic basalts in southern South China Block support the flat-slab subduction model. Lithos 132-133: 127-140.

Middlemost, E.A.K., 1994. Naming materials in the magma/igneous rock system. Earth Science Review 37: 215-224.

Middlemost, E.A.K., 1997. Magmas, rocks and planetary development. Longman, pp 299.

Moyen, J.-F., 2009. High Sr/Y and La/Yb ratios: The meaning of the “adakitic signature”. Lithos 112, 556-574.

Niu, Y.L., 2014. Geological understanding of plate tectonics: Basic concepts, illustrations, examples and new perspectives. Global Tectonics and Metallogeny 10, 1-24.

Oncken, O., Chong, G., Franz, G., Giese, P., Götze, H.J., Ramos, V.A., Strecker, M.R., Wigger, P., 2006. The Andes: Active Subduction Orogeny. Springer, pp 569.

Patiño Douce, A.E., 1997. Generation of metaluminous A-type granites by low-pressure melting of calc-alkaline granitoids. Geology 25, 743-746.

Pearce, J.A., 2008. Geochemical fingerprinting of oceanic basalts with applications to ophiolite classification and the search for Archean oceanic crust. Lithos 100, 14-48.

Petford, N., Gallagher, K., 2001. Partial melting of mafic (amphibolitic) lower crust by periodic influx of basaltic magma. Earth and Planetary Science Letters 193, 483-499.

Qiu, J.S., Li, Z., Liu, L., Zhao, J.L., 2012. Petrogenesis of the Zhangpu composite Granite pluton in Fujian Province: Constraints from zircon U-Pb ages, elemental geochemistry and Nd-Hf isotopes. Acta Geologica Sinica 86, 561-576 (in Chinese with English abstract).

Qiu, J.S., Wang, D.Z., McInnes, B.I.A., 1999. Geochemistry and petrogenesis of the I- and A-type composite granite masses in the coastal area of Zhejiang and Fujian Province. Acta Geologica Sinica 15, 237-246 (in Chinese with English abstract).

Qiu, J.S., Wang, D.Z., Kanisawa, W., McInnes, B.I.A., 2000.Geochemistry and petrogenesis of aluminous A-type granites in the coastal area of Fujian Province. Geochimica 29, 313-321 (in Chinese with English abstract).

Richards, J., Kerrich, R., 2007. Adakite-like rocks: their diverse origins and questionable role in metallogenesis. Economic Geology102, 537-576.

Rickwood, P.C., 1989. Boundary lines within petrologic diagrams which use oxides of major and minor elements. Lithos 22, 247-263.

Roderíguez, C., Sellés, D., Dungan, M., Langmuir, C., Leeman, W., 2007. Adakitic dacites formed by intracrustal crystal fractionation of water-rich parent magmas at Nevadode Longaví Volcano (36.2°S; Andean Southern Volcanic Zone, Central Chile). Journal of Petrology 48, 2033–2061.

Rudnick, R.L., Fountain, D.M., 1995. Nature and composition of the continental crust — a lower crustal perspective. Reviews of Geophysics 33,267-309.

Rudnick, R.L., Gao, S., Ling, W.L., Liu, Y.S., McDonough, W.F., 2004. Petrology and geochemistry of spinel peridotite xenoliths from Hannuoba and Qixia, North China craton. Lithos 77, 609-637.

Shi, J.J., Zhang, S.Z., 2010. Characters of the Mesozoic tectonic activity and geotectonic setting of the Changle-Nan'ao fault zone. Journal of Jilin University (Earth Science Edition) 40, 1333-1343.

Sheppard, S., Griffin, T., Tyler, I., Page, R., 2001. High-and low-K granites and adakites at a Palaeoproterozoic plate boundary in northwestern Australia. Journal of the Geological Society 158, 547-560.

Shu, L.S., Zhou, X.M., Deng, P., Wang, B., Jiang, S.Y., Yu, J.H., Zhao, X.X., 2009. Mesozoic tectonic evolution of the Southeast China Block: New insights from basin analysis. Journal of Asian Earth Sciences 34, 376-391.

Song, S., Su, L., Li, X.-H., Zhang, G., Niu, Y., Zhang, L., 2010. Tracing the 850-Macontinental flood basalts from a piece of subducted continental crust in the North Qaidam UHPM belt, NW China. Precambrian Research 183, 805-816.

Sun, S.S., McDonough, W.F., 1989. Chemical and isotope systematics of oceanic basalts: implications for mantle composition and processes. In: Saunders, A.D., ed. Magmatism in

Ocean Basins. Special Publication, Geological Society of London 42: 313-345.

Tong, W.X., Tobisch, O.T., 1996. Deformation of granitoid plutons in the Dongshan area, Southeast China: constraints on the physical conditions and timing of movement along the Changle-Nan'ao shear zone. Tectonophysics 267, 303-316.

Wang, Z.H., Lu, H.F., 1997. Evidence and dynamics for the change of strike-slip directionof the Changle-Nan'ao ductile shear zone, southeastern China. Journal of Asian Earth Sciences 15, 507-515.

Wang, Z.H., Lu, H.F., 2000. Ductile deformation and $^{40}Ar/^{39}Ar$ dating of the Changle-Nan'ao ductile shear zone, southeastern China. Journal of Structural Geology 22, 561-570.

Wang, D.Z., Shu, L.S., 2012. Late Mesozoic basin and range tectonics and related magmatism in Southeast China. Geoscience Frontiers 3, 109-124.

Wang, Q., McDermott, F., Xu, J.F., Bellon, H., Zhu, Y.T., 2005. Cenozoic K-rich adakitic volcanic rocks in the Hohxil area, northern Tibet: lower-crustal melting in an intracontinental setting. Geology 33, 465–468.

Wang, Y.J., Fan, W.M., Zhang, G.W., Zhang, Y.H., 2013. Phanerozoic tectonics of the South China Block: Key observations and controversies. Gondwana Research 23, 1273–1305.

Wiebe, R.A., 1991. Commingling of contrasted magmas and generation of mafic enclaves in granitic rocks. In: Didier, J., Barbarin, B. (Eds.), Enclaves and Granite Petrology, Elsevier, Amsterdam, 625p.

Wiedenbeck, M., Alle, P., Corfu, F., Griffin, W.L., Meier, M., Oberli, F., Quadt, A.V., Roddick, J.C., Spiegel, W., 1995. Three natural zircon standards for U-Th-Pb, Lu-Hf, trace element and REE analyses. Geostandards and Geoanalytical Research 19, 1-23.

Wolf, M.B., London, D., 1994. Apatite dissolution into peraluminous haplogranite melts: An

experimental study of solubilities and mechanisms. Geochimica et Cosmochimica Acta 58, 4127-4145.

Woodhead, J., Hergt, J., Shelley, M., Eggins, S., Kemp, R., 2004. Zircon Hf-isotope analysis with an excimer laser, depth profiling, ablation of complex geometries, and concomitant age estimation. Chemical Geology 209: 121-135.

Wu, F.Y., Jahn, B.M., Wilde, S., Sun, D.Y., 2000. Phanerozoic crustal growth: U-Pb and Sr-Nd isotopic evidence from the granites in northeastern China. Tectonophysics 328, 89-113.

Wu, F.Y., Jahn, B.M., Lo, C.H., Yui, T.F., Lin, Q., Ge, W.C., Sun, D.Y., 2003. Highly fractionated I-type granites in NE China (I): geochronology and petrogenesis. Lithos 66, 241-273.

Wu, F.Y., Li, X.H., Yang, J.H., Zheng, Y.F., 2007. Discussions on the petrogenesis of granites. Acta Ptrologica Sinica 23 (6), 1217-1238 (in Chinese with English abstract).

Xu, H.J., Ma, C.Q., Zhang, J.F., 2012. Generation of Early Cretaceous High-Mg adakitic host and enclaves by magma mixing, Dabie orogen, Eastern China. Lithos 142–143, 182–200.

Yang, J.B., Sheng, D., Zhao, Z.D., Ding, C., Zhou, H.F., Cui, Y.Y., Jiang, T., Hu, Z.C., 2013. Petrogenesis and implications of granites and associated dioritic enclaves in Jiaomei area, Zhangzhou, Fujian Province. Acta Petrologica Sinica 29 (11), 4004-4010 (in Chinese with English abstract).

Yang, Y.F., Dong, C.W., Yan, Q., Li, N.M., Zhu, G.Q., Song, Y.Q., 2010a. Late Mesozoic extension in the coastal area of Zhejiang and Fujian Province: an indicator from the basic-intermediate dykes, coastland of Fujian Province. Journal of Mineralogy and Petrology 30, 87-94 (in Chinese with English abstract).

Yang, Y.F., Yang, J.J., Li, N.M., Yan, Q., Zhan, X., Dong, C.W., 2010b. SHRIMP U-Pb zircon dating of the basic-intermediate dykes from the coastland of Fujian Province, Geological Science

and Technology Information 29 (5), 23-29 (in Chinese with English abstract).

Yin, A., 2010. Cenozoic tectonic evolution of Asia: A preliminary synthesis. Tectonophysics 488, 293-325.

Yu, J.H., Xu, X.S., Zhou, X.M., 2003. Late Mesozoic crust-mantle interaction and lower crust components in South China: A geochemical study of mafic granulite xenoliths from Cenozoic basalts. Science in China Series D: Earth Sciences 46, 447-460.

Zhao, D., 2004a. Global tomographic images of mantle plumes and subducting slabs: insight into deep Earth dynamics. Physics of the Earth and Planetary Interiors 146, 3-34.

Zhao, J.H., 2004b. Chronology and geochemistry of mafic rocks from Fujian Province: implications for the mantle evolution of SE China since Late Mesozoic. A dissertation submitted for the degree of Doctor of Philosophy, Institute of Geochemistry of Chinese Academy of Sciences, Guiyang, China, pp. 1-107 (in Chinese with English abstract).

Zhao, J.L., Qiu, J.S., Li, Z., Liu, L., Li, Y.L., 2012. Petrogenesis of the Taiwushan granite pluton in Fujian Province: Constraints from zircon U-Pb ages and Hf isotopes. Acta Petrologica Sinica 28 (12), 3938-3950 (in Chinese with English abstract).

Zheng, J.P., O'Reilly, S.Y., Griffin, W.L., Zhang, M., Lu, F.X., Liu, G.L., 2004. Nature and evolution of Mesozoic-Cenozoic lithospheric mantle beneath the Cathaysia block, SE China. Lithos 74, 41-65.

Zhou, J.C., Chen, R., 2001. Geochemistry of late Mesozoic interaction between crust and mantle in southeastern Fujian Province. Geochimica 30, 547-558.

Zhou, X.M., Li, W.X., 2000. Origin of Late Mesozoic igneous rocks of southeastern China: implications for lithosphere subduction and underplating of mafic magma. Tectonophysics 326, 269-287.

Zhou, X.M., Sun, T., Shen, W.Z., Shu, L.S., Niu, Y.L., 2006. Petrogenesis of Mesozoic granitoids and volcanic rocks in South China: A response to tectonic evolution. Episodes 29, 26-33.

Zhou, X.M., 2007. Genesis of Late Mesozoic Granitoids in the Nanling Region and the Lithospheric Dynamic Evolution. Science Press, Beijing, pp. 1-691 (in Chinese with English abstract).

Zorpi, M.J., Coulon, C., Orsini J.B., Cocirta, C., 1989. Magma mingling, zoning and emplacement in calc-alkaline granitoid plutons. Tectonophysics 157, 315-329.

Zorpi, M.J., Coulon, C., Orsini J.B., 1991. Hybridization between felsic and mafic magmas in calc-alkaline granitoids—a case study in northern Sardinia, Italy. In: Peccerillo, A. (Guest-Editor), Geochemistry of Granitoid Rocks. Chemical Geology 92, 45-86.

Figure captions

Fig. 1. Geological map of Mesozoic granitic and volcanic rocks, and tectonic features in South China (modified after Zhou *et al.*, 2006; Shu *et al.*, 2009; Wang and Shu, 2012; Zheng *et al.*, 2004). SJPF: Shaoxing-Jiangshan-Pingxiang Fault Zone; CNF: Changle-Nan'ao Fault Zone; ZDF: Zhenghe-Dapu Fault Zone; GXF: Guangchang-Xunwu Fault Zone; GF: Ganjiang Fault Zone; SWF: Sihui-Wuchuan Fault Zone; NJF: Ningyuan-Jianghua Fault Zone.

Fig. 2. Simplified geological maps of Quanzhou (a) and Xiamen (b), showing the distribution of Cretaceous granites, sample locations (blue stars), U-Pb zircon ages of igneous rocks (ovals with numerals, italic for dyke dating), and major northeast-trending faults and felsic dykes. (c) Intermediate dykes intruding with near-vertical orientation into a granite pluton (in Xiamen). (d) Dykes mutually cross-cutting with clear boundaries (in Quanzhou).

Fig. 3. Photomicrographs (crossed polars) of thin-sections from granites and intermediate dykes. Indices: Bi: biotite; Cal: calcite; Cpx: clinopyroxene; Hbl: hornblende; Kfs: K-feldspar; Ms: muscovite; Per: perthite; Pl: plagioclase; Q: quartz; San: sanidine.

Fig. 4. Representative Cathodoluminescence (CL) images of zircon grains and LA-ICP-MS U-Pb Concordia diagrams for Cretaceous granites and intermediate dykes in Quanzhou and Xiamen. Plots (d), (e) and (l) are dates for intermediate dykes, others are for granites. The solid (32 μm) and dashed (44 μm) circles respectively indicate the locations of LA-ICP-MS U-Pb and Hf isotopic analyses. The scale bar in all CL images is 100 μm in length.

Fig. 5. Plots of (a) (Na_2O+K_2O) versus SiO_2, (b) K_2O versus $SiO_2$and (c) A/NK [molar ratio $Al_2O_3/(Na_2O+K_2O)$] versus A/CNK [molar ratio $Al_2O_3/(CaO+Na_2O+K_2O)$] for Cretaceous granites and intermediate dykes in coastal Fujian Province. Diagrams (a), (b) and (c) are respectively from Middlemost (1994), Rickwood (1989), and Maniar and Piccoli (1989). Green and red crosses respectively represent previously published data of Mesozoic basic-intermediate plutons/dykes and granites from coastal Fujian Province (refer to Supplementary Data and Appendix). Indices: FG: Foid Gabbro; FMd: Foid Monzodiorite; FMs: Foid Monzosyenite; GD: Gabbroic Diorite; Md: Monzodiorite.

Fig. 6. Chondrite-normalised REE (a, c and e) and primitive mantle (PM) normalised trace element (b, d and f) patterns for Cretaceous granites and intermediate dykes in coastal Fujian Province. The values of OIB, E-MORB, N-MORB, chondrite and primitive mantle are from Sun and McDonough (1989), and shown as the grey fields (refer to Supplementary Data and Appendix).

Fig. 7. (a) Bulk-rock $\varepsilon_{Nd}(t)$ versus $(^{87}Sr/^{86}Sr)_i$ diagram for Cretaceous granites and basic-intermediate dykes/plutons in coastal Fujian Province. (b) Zircon $\varepsilon_{Hf}(t)$ versus U-Pb ages diagram for Cretaceous granites and basic-intermediate dykes/plutons in coastal Fujian Province. CBGX: Cumulate basic granulite xenoliths; MBGX: Magmatic basic granulite xenoliths. (c) and (d) Zircon Hf model ages versus U-Pb ages diagrams for Cretaceous granites and basic-intermediate dykes/plutons in coastal Fujian Province. The approximate field of Cainozoic basalts in SE China is from Chen *et al*. 2014. Basic granulite xenolith data are from Yu *et al*. 2003. Green and red crosses respectively represent previously published data of

Mesozoic basic-intermediate plutons/dykes, and granites from coastal Fujian Province (refer to Supplementary Data and Appendix).

Fig. 8. Simplified spatial-temporal map of Cretaceous intrusive magmatism in coastal Fujian Province (modified after Li *et al.*, 2014 and Zhou *et al.*, 2006), previously published data with numbers in brackets are listed in Supplementary Data. Red ages for I-type granites, dark blue ages for A-type granites, and green ages for basic-intermediate rocks.

Fig. 9. FeO*/MgO versus SiO_2 (a) (Eby, 1990), P_2O_5 versus SiO_2 (b), and plots of Y (c), Th (d) against Rb (Chappell, 1999) discriminant diagrams for Cretaceous granites in coastal Fujian Province. Red crosses represent previously published data of Mesozoic granites from coastal Fujian Province (refer to Supplementary Data and Appendix).

Fig. 10. Harker diagrams of selected major elements for Cretaceous intermediate dykes in Quanzhou and Xiamen.

Fig. 11. Nb/Ta versus Zr/Sm (Foly *et al.*, 2002) (a), Th/Yb versus Nb/Yb (Pearce, 2008) (b), FeO* versus MgO (Zorpi *et al.*, 1989; 1991) (c) and (Sr/Y) versus Y (Defant and Drummond, 1990) (d) diagrams for Cretaceous granites and intermediate dykes in coastal Fujian Province. In (b): N-MORB, E-MORB, OIB and Primitive Mantle (PM) are from Sun and McDonough (1989); average lower crust (LC), upper crust (UC), Middle crust (MC) and total continental crust (CC) are from Rudnick and Fountain (1995). Green and red crosses represent previously published data of Mesozoic basic-intermediate plutons/dykes, and granites from coastal

Fujian Province (refer to Supplementary Data and Appendix). Adakitic rock data are listed in the trace elements sheets of Supplementary Data.

Fig. 12. Simplified model cross-sections for Cretaceous subduction dynamics of the Palaeo-Pacific slab under the Cathaysia Plate.

Yang et al. Figure 1 W 170 mm × H 145 mm

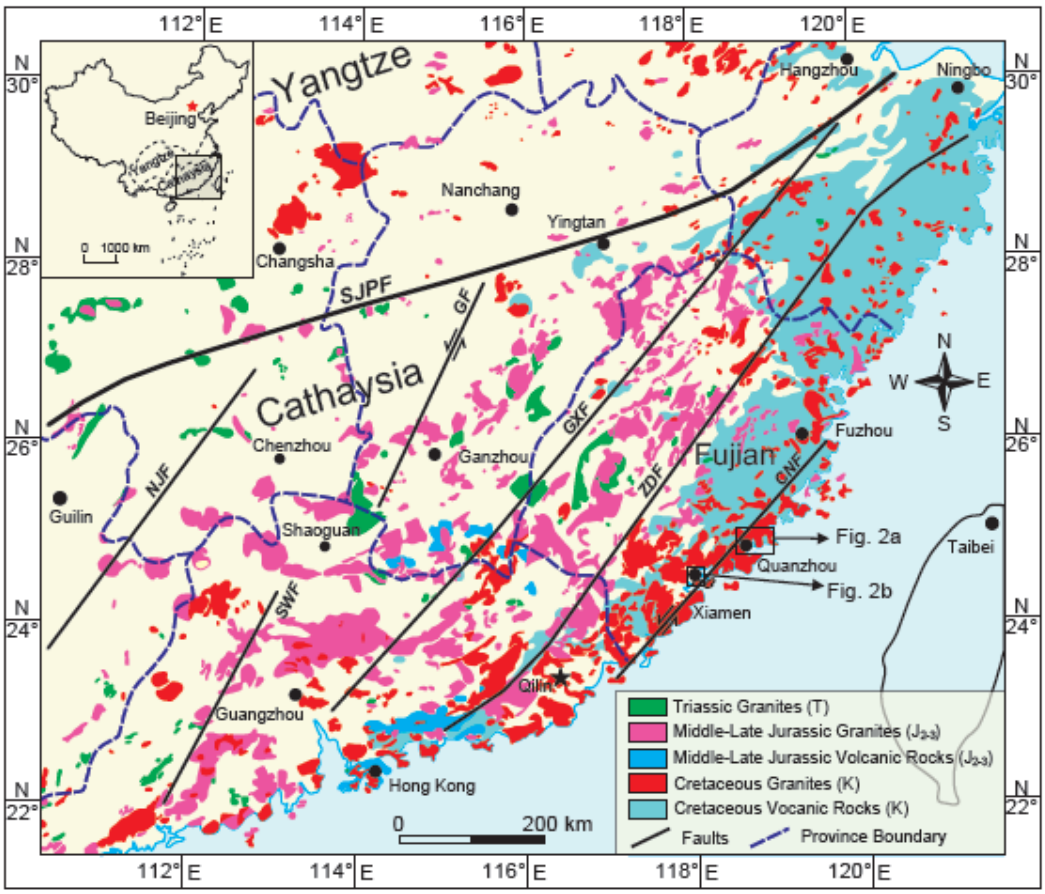

Yang et al. Figure 2 W 179 mm × H 244 mm

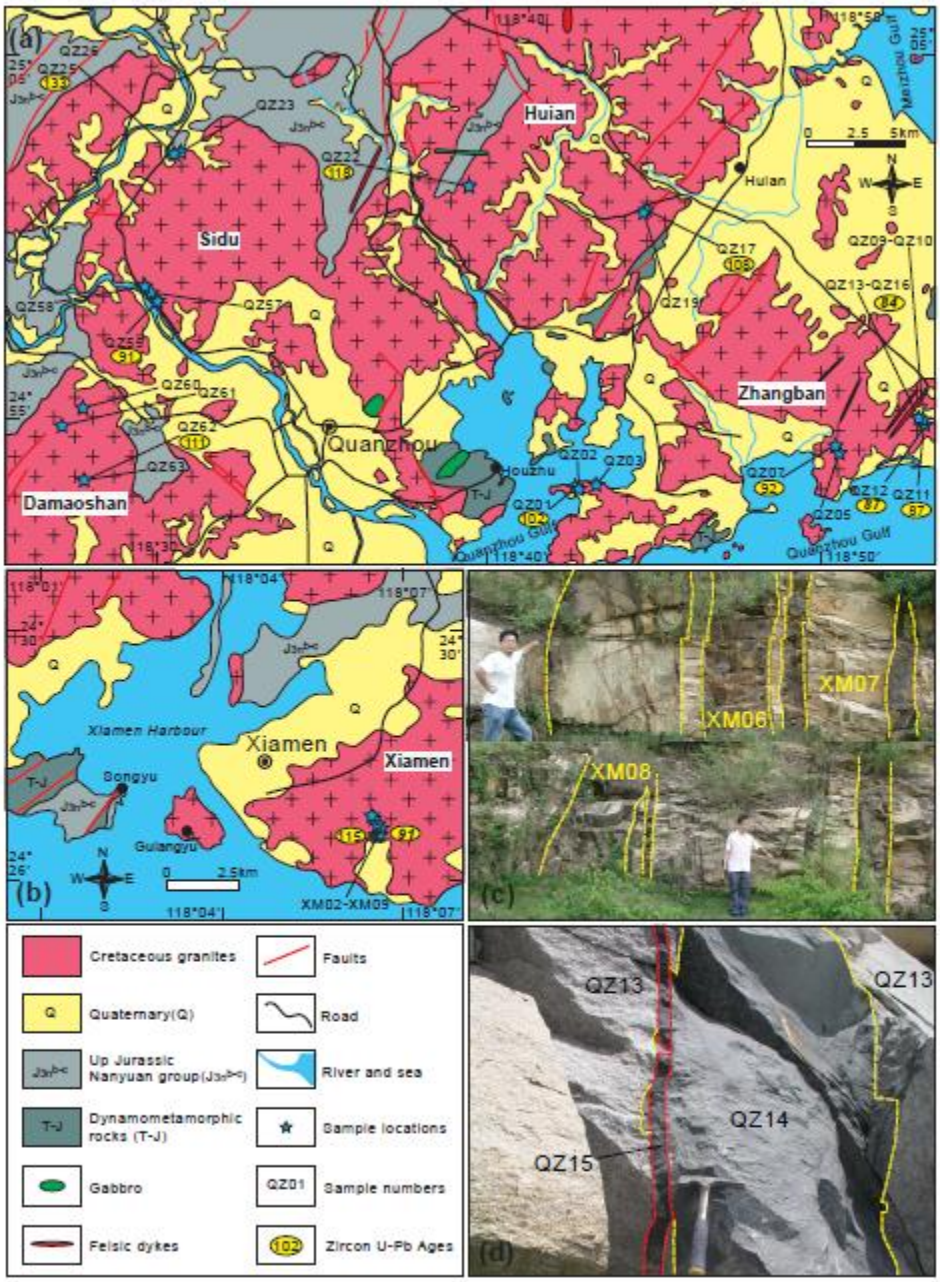

Yang et al. Figure 3 W 167 mm × H 188 mm

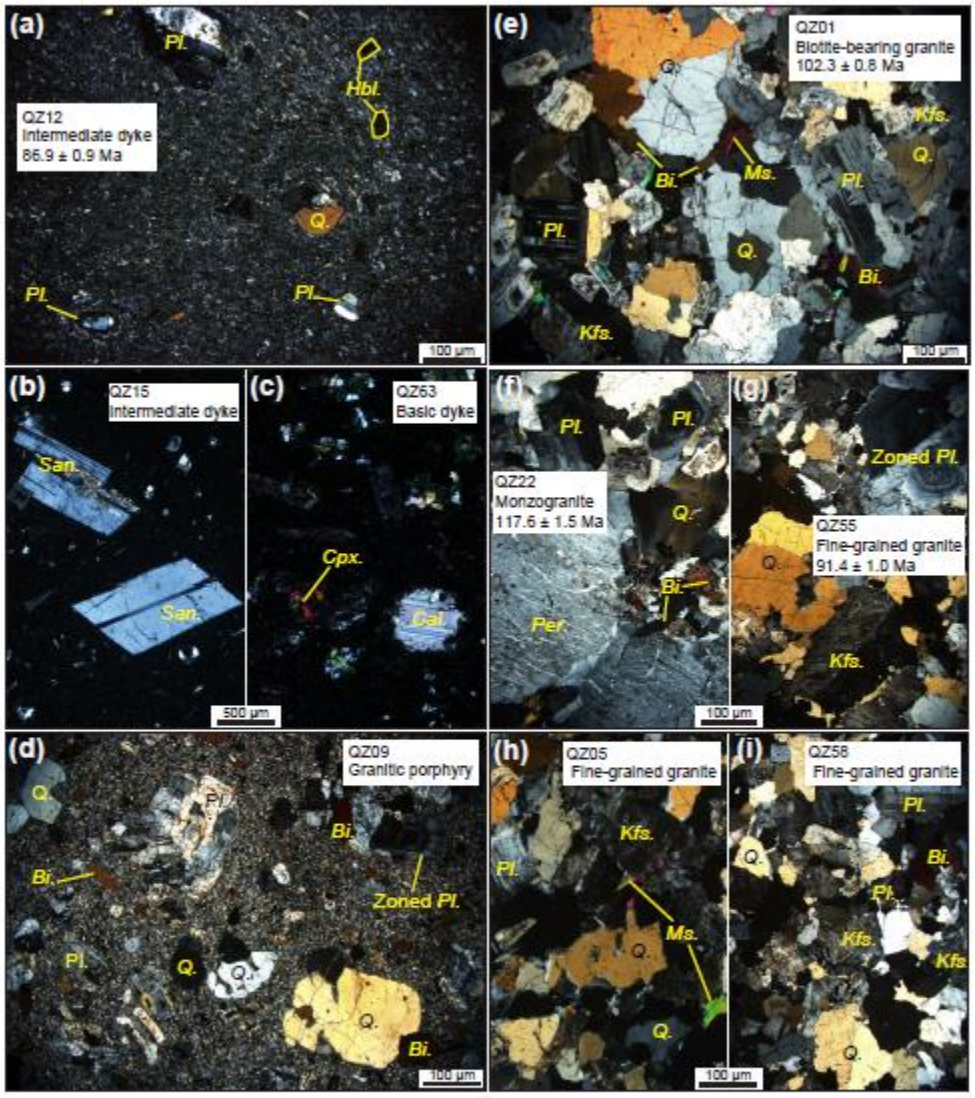

Yang et al. Figure 4 W 179 mm × H 188 mm

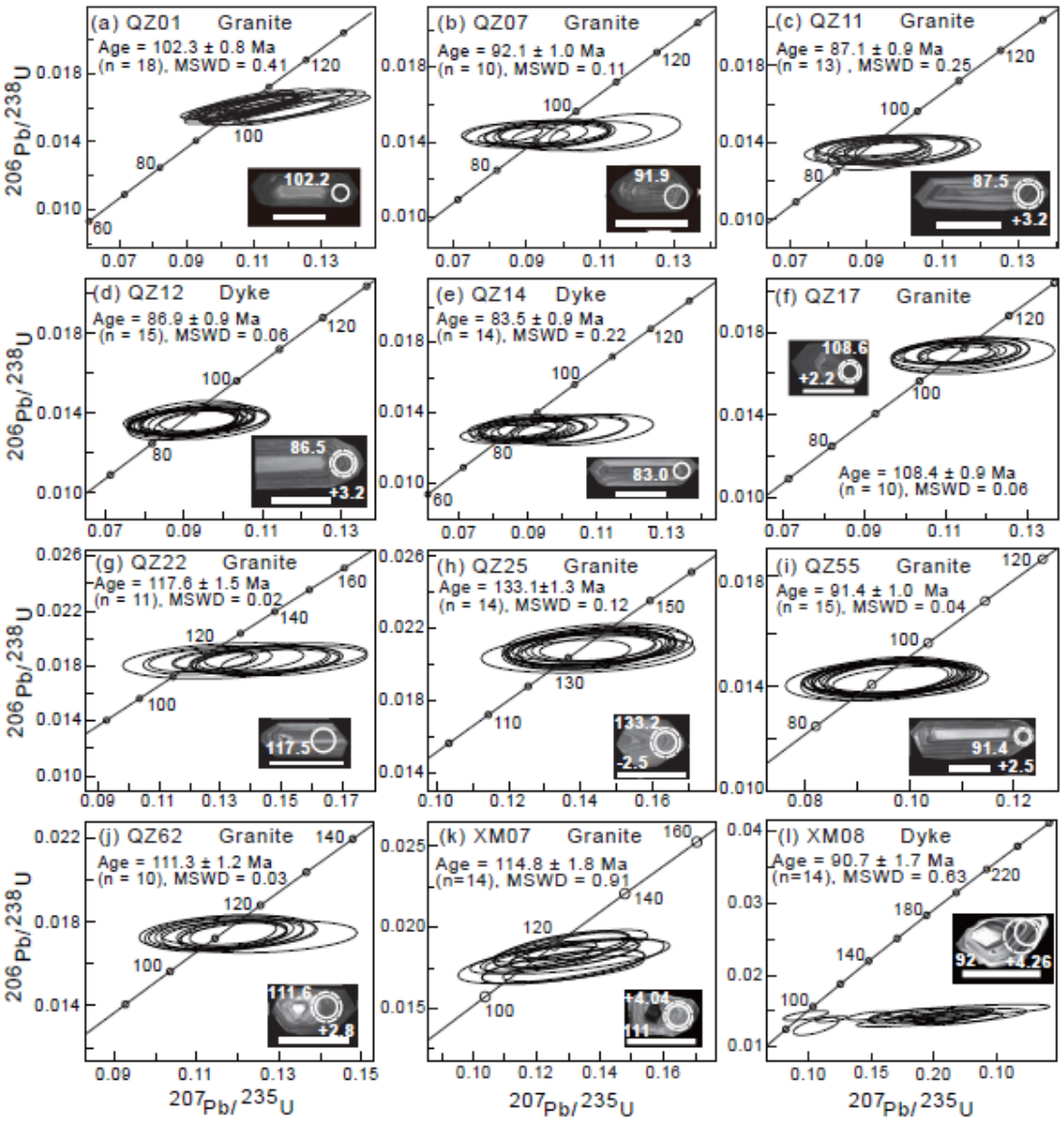

Yang et al. Figure 5 W 84 mm × H 194 mm

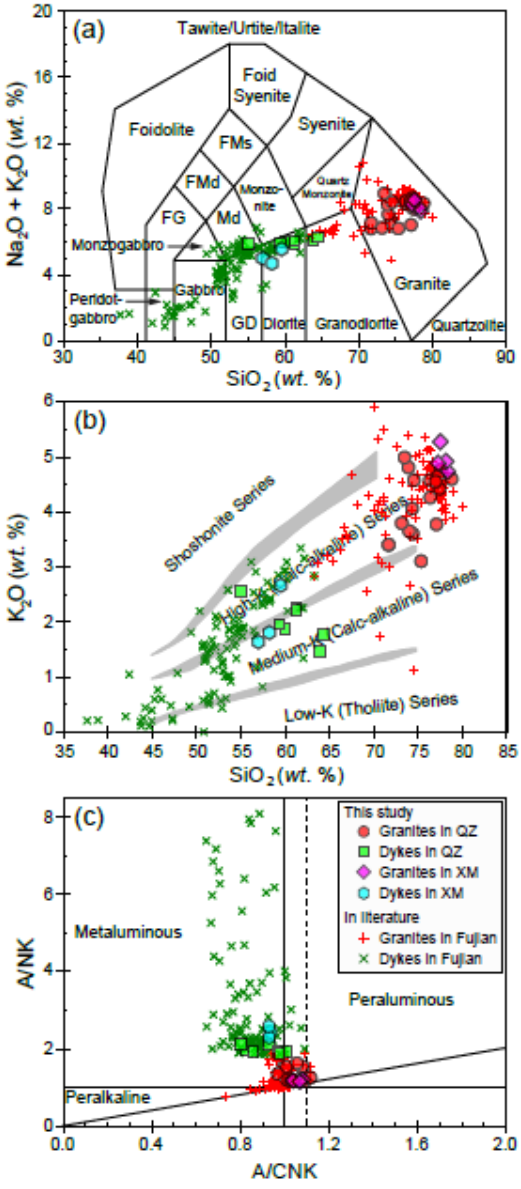

Yang et al. Figure 6 W 165 mm × H 160 mm

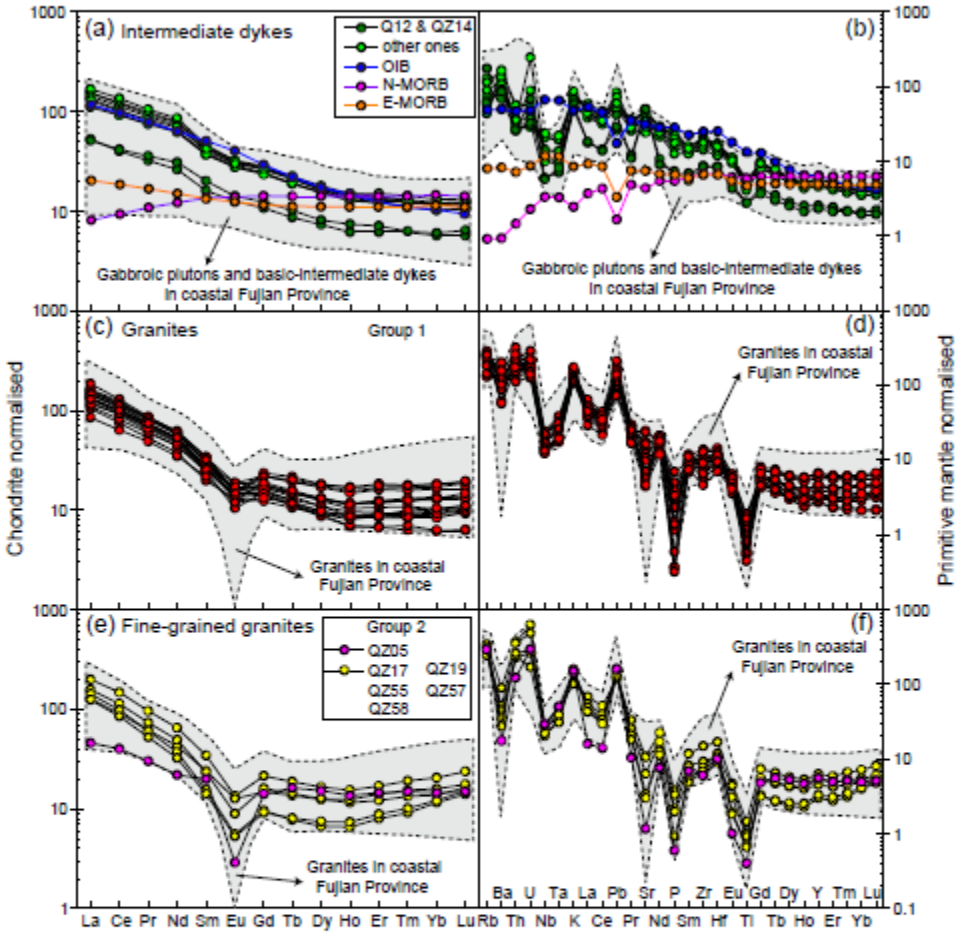

Yang et al. Figure 7 W 167 mm × H 131 mm

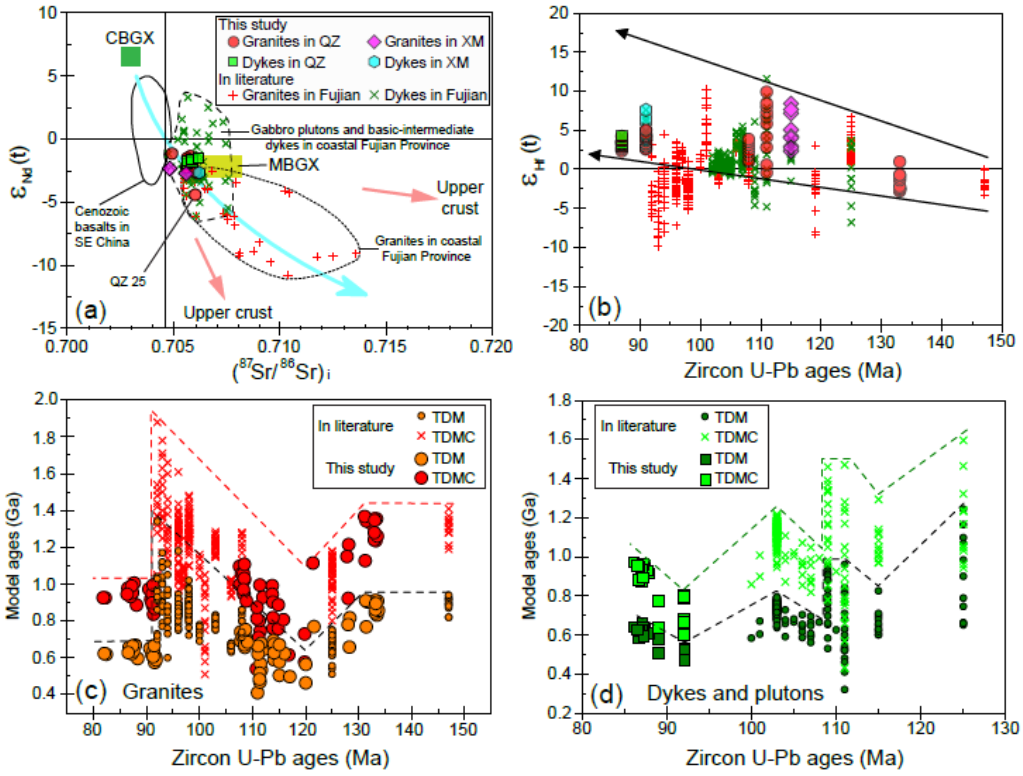

Yang et al. Figure 8 W 165 mm × H 114 mm

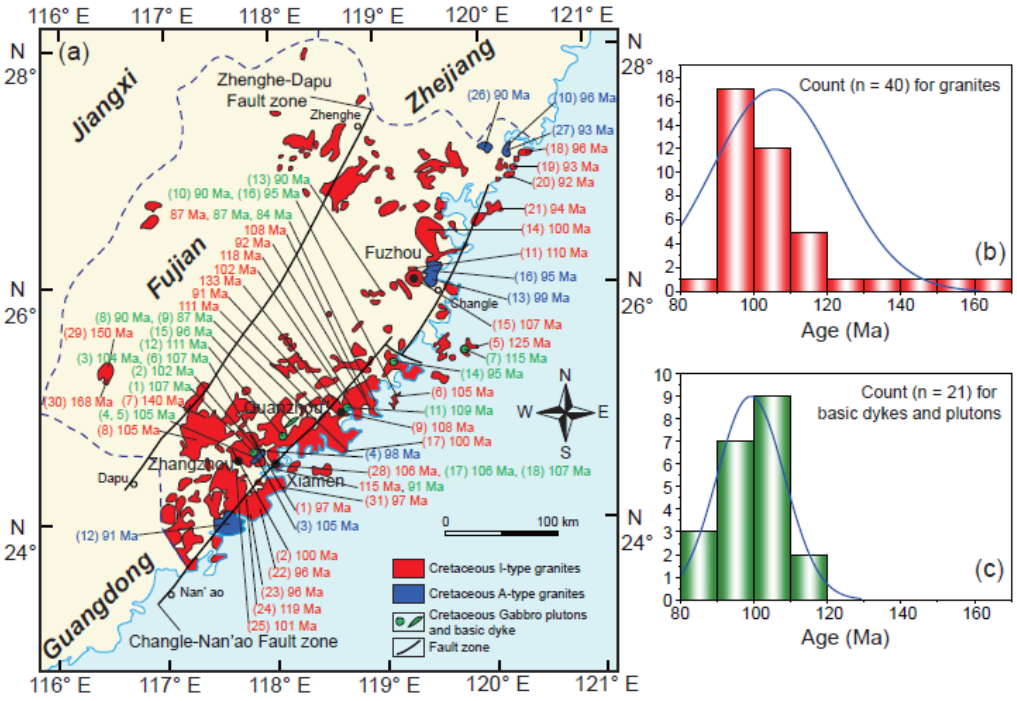

Yang et al. Figure 9 W 165 mm × H 123 mm

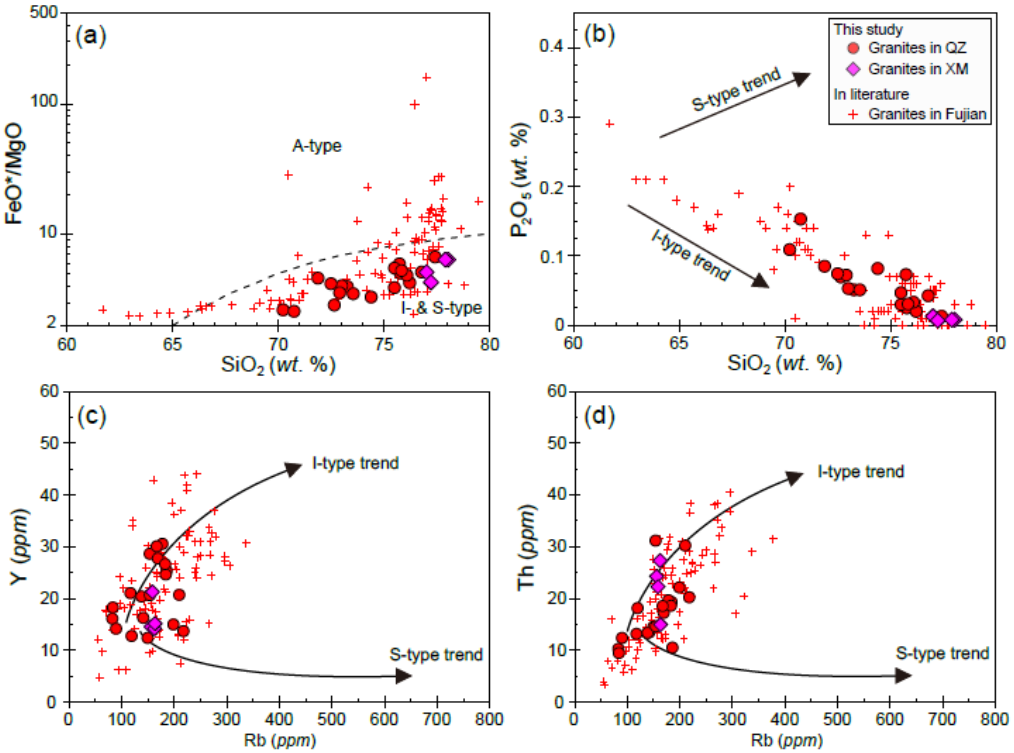

Yang et al. Figure 10 W 160 mm × H 120 mm

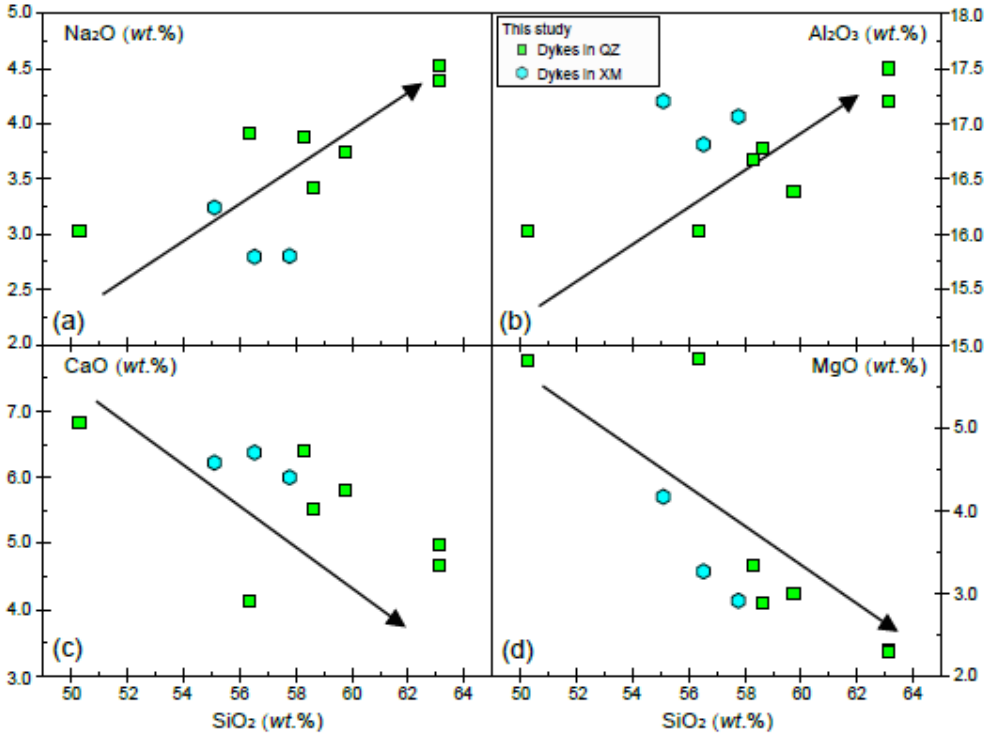

Yang et al. Figure 11 W 163 mm × H 123 mm

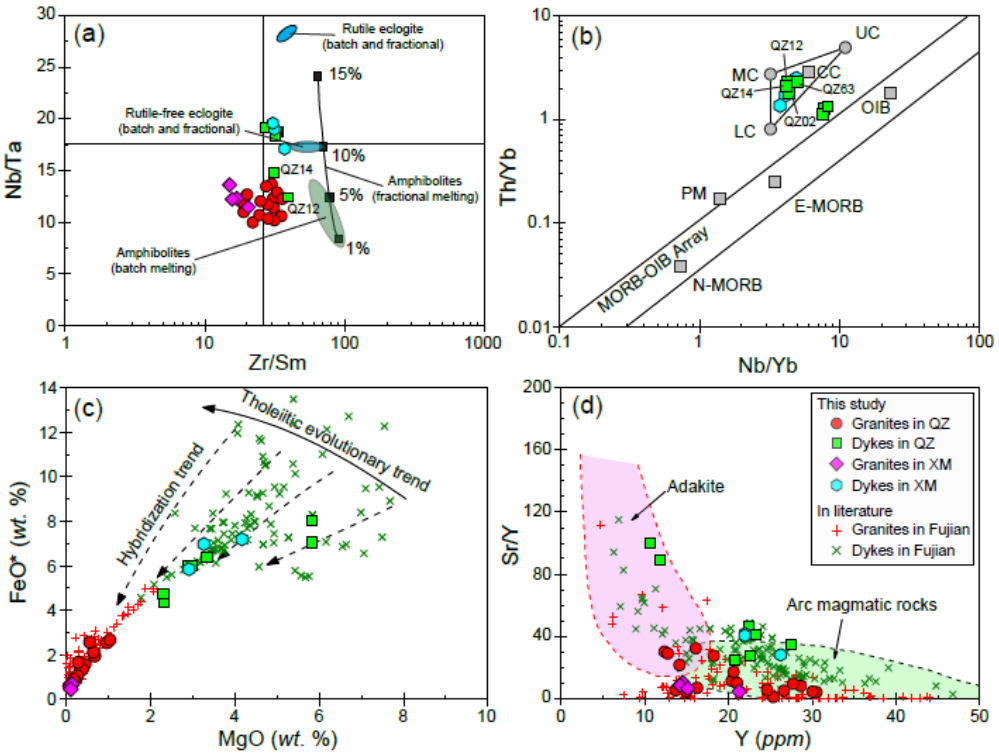

Yang et al. Fig. 12 W 126 × H 123

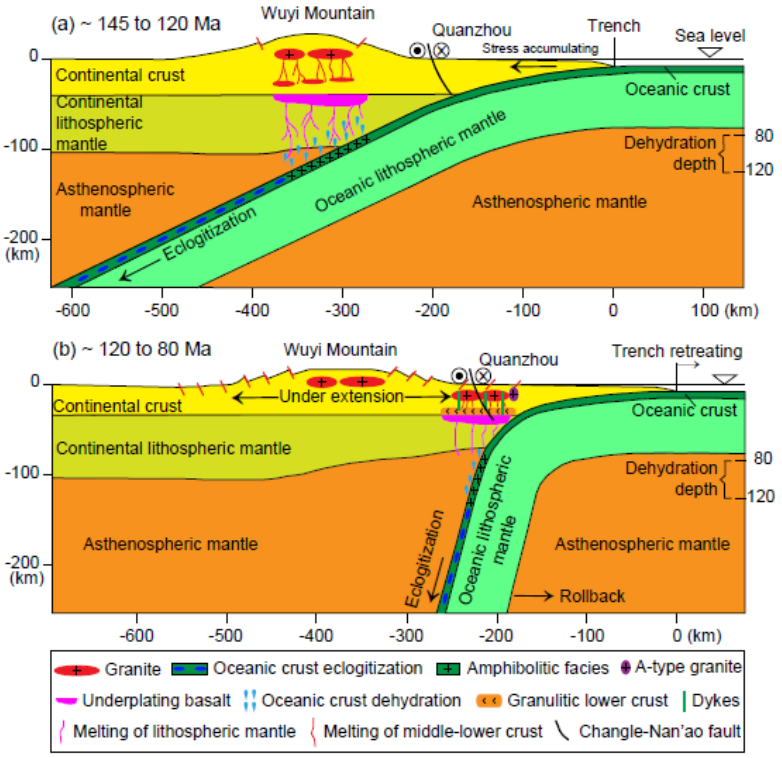

Highlights

1. Twelve new zircon U-Pb ages of 133–84 Ma become younger from inland to coast.
2. The granites crystallised as I type and derived from middle-lower crust.
3. Eight intermediate dykes derived from residual basic lower crust after accumulation.
4. Two adakite-like dykes derived from a mixed lower crust source.
5. Subduction retreat was principal style of Cretaceous Palaeo-Pacific slab subduction.